Bulletin of Mathematical Biology (2026) 88:197
https://doi.org/10.1007/s11538-026-01763-8

Society for Mathematical Biology

UNSOLVED PROBLEMS



A Comparison of Mechanisms Driving Lesion Outcomes During Lung Tumor and Tuberculosis Granuloma Formation

Christian T. Michael[1] · **Maral Budak**[1] · **Denise Kirschner**[1]

Received: 26 February 2026 / Accepted: 14 September 2026
© The Author(s) 2026

Abstract

Small cell lung cancer (SCLC) and tuberculosis (TB) are both deadly diseases that present with spatially complex lung lesions. These lesions share similarities, including spatial interactions between T cells and macrophages. Both SCLC and TB exhibit heterogeneous disease progression and responses to treatment; current experimental methods have few tools to investigate the spatiotemporal evolution of these lesions within human lungs. We have applied our computational agent-based model (ABM), *GranSim*, to extensively study heterogeneity of TB granuloma formation and treatment efficacy. We introduce *TumorSim*, an analogous ABM designed to understand heterogeneity of SCLC lung tumors. *TumorSim* mechanistically captures immune-tumor interactions, many of which are well-studied in isolation, including cytokine-based recruitment of immune cells and PD-1/PD-L1-based inhibition of cytotoxic T cells. Drawing from lung immunology literature, we define and explore wide parameter ranges to characterize *TumorSim* behavior using global sensitivity analysis. We compare factors that drive both tumor and granuloma outcomes. As model validation, sensitivity analysis captures several well-known correlates of improved SCLC outcomes including macrophage-mediated cytotoxic T-cell recruitment. Surprisingly, both models predict a two-phase formation process occurring with an abrupt change in tumor/granuloma dynamics upon arrival of adaptive immune cells into the lung. Simulations suggest that while C–C motif chemokine ligand 5 (CCL5) is associated with improved tumor control later during tumor growth, CCL5 plays a pro-tumor role early during tumor growth by recruiting regulatory T cells. We find that, like virtual granulomas, *TumorSim* tumors become enlarged when immunosuppressive mechanisms outweigh pro-inflammatory responses. This novel tumor model enables future studies of both immunotherapeutics and anti-cancer drugs.

Keywords Small-cell lung cancer · agent-based models

✉ Denise Kirschner
kirschne@umich.edu

[1] Kirschner Lab, Department of Microbiology & Immunology, University of Michigan - Michigan Medicine, Ann Arbor, MI, USA

Published online: 06 October 2026

1 Introduction

Small cell lung cancer (SCLC) and pulmonary Tuberculosis (TB), two leading causes of death worldwide, both manifest in lungs with lesions that share anatomic and functional similarities that directly impact disease progression and responses to therapies. SCLC, an aggressive form of lung cancer with a $< 7\%$ five-year survival, accounts for about 15% of lung cancer cases (Zhong et al., 2026). TB is a bacterial disease caused by infection with *Mycobacterium tuberculosis* (Mtb), and is the world's leading cause of death by a single infectious pathogen and has been for decades (World Health Organization 2025). Discrete lung masses form in and on lung stroma during both SCLC and pulmonary Mtb infection, and in each disease these masses result from recruitment of multiple, overlapping immune cells to both lesions and their ensuing complex interactions. In fact, due to the similarities between TB and SCLC, TB patients are often misdiagnosed with lung cancer based on PET-CT scans in regions with high TB incidence (Low et al. 2006; Werutsky et al. 2019). Moreover, many studies have provided evidence that patients with TB have an increased risk of lung cancer (Wu et al. 2011; Yu et al. 2011; Ho et al. 2021; Fang et al. 2025). Treatment of both SCLC and TB presents formidable challenges necessitating multi-drug regimens designed to overcome heterogeneous spatial drug delivery and pre-existing and/or acquired drug resistance. While effective (though intensive and expensive) treatment for TB exists (Saukkonen et al. 2025), current therapies for SCLC fail for many patients (Li et al. 2022; Kim et al. 2025), emphasizing the need for us to better understand basic immunological mechanisms and drivers of tumor heterogeneity. A mechanistic computational model can help identify these factors.

Lung cancer, especially SCLC, has many features in common with TB. TB granulomas and lung cancer lesions pose remarkably similar challenges to disease elimination via immune response or treatment (Fig. 1). In both, an effective immune response is impaired in the lung microenvironment due to increased immunosuppressive cells (myeloid-derived suppressor cells or regulatory T cells) or T-cell exhaustion (Whiteside 2008; Wang et al. 2019; Ashenafi et al. 2022). Spatially-heterogeneous architectures of granulomas and tumors, including poorly developed vasculature and distorted extracellular matrix, impair drug delivery and T-cell infiltration into both types of lesions (Sarathy et al. 2016; Peranzoni et al. 2018; Millar et al. 2020). The resulting heterogeneous distribution of drugs throughout lesions contributes towards the commonly-observed outcomes of drug resistance and subsequent treatment failure, especially in combination with pre-existing or acquired mutations in granulomas/tumors due to nutrient-poor lesion microenvironments (Ormerod 2005; Wu et al. 2014). These challenges necessitate extended courses of treatments for both diseases with multiple drugs (Bayat Mokhtari et al. 2017; Kerantzas et al. 2017).

TB lung granulomas and lung tumors share anatomic and functional similarities that directly impact disease progression and response to therapy (Fang et al. 2025). In response to infection with Mtb or formation of cancer cells, the host recruits a wide variety of immune cells, including effector and immunosuppressive myeloid lineage cells and T lymphocytes, and other stromal cell types such as activated fibroblasts. This results in the emergence of complex and spatially heterogeneous structures called granulomas (TB) or solid tumors (cancer) (Fig. 1) (Bickett et al. 2020; Dorhoi et al.

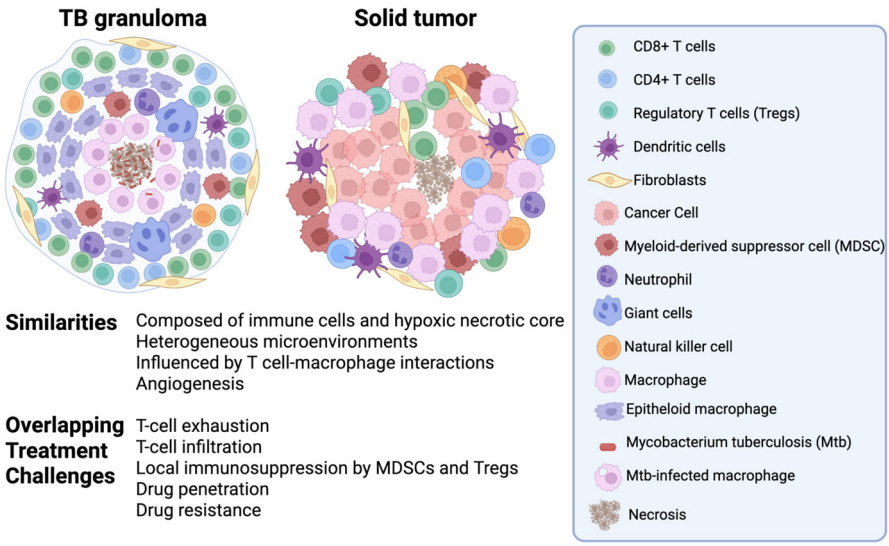


Fig. 1 Summary comparison of tuberculosis (TB) granuloma and solid tumor lesion microenvironments. These cartoons depict the typical presentations of SCLC and TB. Granulomas are approximately spherical (Ramakrishnan 2012), while SCLC tumors tend to be lobular once diagnosed (Travis 2012), likely shaped by the stromal architecture. We thus assume that for small, early tumors, a sphere is a reasonable approximation. Both lesions comprise multiple types of immune cells clustering around Mtb infection and neoplasm, respectively. Initial interaction between macrophages and dendritic cells results in the recruitment of an adaptive immune response. Activity of apoptosis-inducing leukocytes (cytotoxic T cells, natural killer cells, pro-inflammatory macrophages) is critical for effective resolution and is hampered by anti-inflammatory leukocytes such as regulatory T cells, anti-inflammatory macrophages, and myeloid-derived suppressor cells (Li et al. 2022; Fang et al. 2025). The core of each lesion is often hypoxic and necrotic (Ramakrishnan 2012; Li et al. 2022). Created in BioRender. Michael, C. (2026) https://BioRender.com/a4s97gv

2020; Ashenafi et al. 2022; Lasser et al. 2024). Host immune responses commonly do not eliminate Mtb or cancer cells, producing two outcomes: (1) progressive disease in either case; or (2) clinical latency (TB) or dormancy (cancer), in which a small number of bacteria or cancer cells remain in a viable, growth-arrested or slowly-dividing state for extended periods of time (Lin et al. 2018; Fabrizio 2025). The course of TB and lung cancer is heavily dependent on the interactions between T lymphocytes and macrophages in lesion microenvironments (Bickett et al. 2020; Ashenafi et al. 2022).

Despite the many cell-scale similarities between SCLC and TB, the two diseases bear several important differences. At its core, cancer is a disease caused by a dysregulation of a host's own cells, thus tumor cells are immune-evasive (i.e., poorly targeted by the immune system), and several recent cancer therapies are aimed at engaging the immune system via exogenous means (Qi et al. 2024; Lowery et al. 2025). When left untreated, SCLC frequently results in large lesions with a very high mortality rate (Wang et al. 2022). By contrast, the human adaptive immune system is relatively efficient at identifying the presence of TB, yet Mtb itself has evolved to inhibit macrophages' ability to digest the bacterium (Ramakrishnan 2012). Consequently,

many macrophages respond to Mtb infection, but the immune system struggles to sterilize infection even once it has been engaged unless the system is activated; the time delay for activation usually means the immune system lags behind bacterial growth, reducing efficacy. Common treatments for TB are combinations of bacteriostatic and bactericidal antibiotics (Bonnett et al. 2017; Cicchese et al. 2020a, b). These and other differences between the two lesions contribute to distinct characteristic time-scales of SCLC and TB, despite the many overlapping cell types and immune mechanisms. SCLC tumors expand quickly largely unchallenged by the immune system, while non-sterile granulomas may linger for years as sites of chronic inflammation (Lin et al. 2014, 2018). Finally, differences in characteristic timescales means that there are no temporally direct comparisons for identifying driving mechanisms of outcomes.

Emergent lung lesions such as tumors and granulomas are challenging to study, as gross predictive power can be elusive despite knowing the myriad of constituent mechanisms and key cell types present. An effective method for identifying principle drivers of clinical outcomes are in silico, mechanistic, multivariate, mathematical models. When calibrated and validated to experimental and clinical datasets, multi-scale models are useful and cost-efficient at capturing complexities of a biological system that may be challenging to probe by experimental methods. We have previously developed a multi-scale mechanistic hybrid agent-based model, *GranSim*, that recapitulates heterogeneous outcomes of lung granuloma progressions, entirely emergent from cell-scale immune responses to pulmonary Mtb infection (Segovia-Juarez et al. 2004; Ray et al. 2009; Fallahi-Sichani et al. 2011; Cilfone et al. 2013). In this work, we create a novel, tandem hybrid agent-based model to understand factors that contribute to lung solid tumor formation and heterogeneity. We introduce a new multi-scale model, *TumorSim*, that captures mechanisms driving SCLC lung tumor formation dynamics. We compare and contrast *TumorSim* to the dynamics of our well-characterized *GranSim* model behavior to investigate similarities and differences between mechanisms of TB and SCLC. Our goal is to harness cross-talk between these two disparate disciplines (infection disease and cancer) that will help foster new ideas and research advancement for both.

2 Methods

To study emergent lesion structures that arise such as SCLC tumors or TB granulomas, we need to explicitly represent cell-and molecular scale details. Several simplified models of tumors exist, though these models focus on large-scale measurements and embed mechanistic hypotheses within the structure of their governing equations (Mohsin et al. 2024). We choose to model both the temporal and spatial aspects of SCLC lung tumors that have been identified as key drivers of lung disease treatment outcomes (Dangaj et al. 2019; Wu et al. 2019; Zheng et al. 2021; Kohli et al. 2022; Li et al. 2022). Agent-based models (ABMs) represent biological systems as collections of interacting *agents* (e.g., cells) that interact to form emergent structures; direct representation allows for mechanistic probing of how smaller-scale agents affect larger-scale outcomes (e.g., tumors and granulomas). ABMs allow for

explicit representation of cell-scale mechanism and modular updates as new information becomes available and have been used for a variety of applications (Cockrell et al. 2017; Ghaffarizadeh et al. 2018; Liu et al. 2021).

Several general ABM frameworks have been developed to generate cell-scale simulations; using these a modeler may follow a straightforward protocol to create a cancer simulation (Poleszczuk et al. 2016). Chaste is a C++ library that provides a platform for rapid and reproducible prototyping of cancer, heart, and soft tissues using center-based, vertex-based, or Cellular-Potts-based architectures (Mirams et al. 2013). Chaste was recently used to study macrophage interactions within the tumor microenvironment (Bull et al. 2023). PhysiCell provides a substantial ecosystem of ABM tools that allow modelers to define rules in human-readable, controlled-vocabulary terms and has been used to simulate a wide variety of biological systems (Ghaffarizadeh et al. 2018). PhysiCell was used to build a high-throughput environment for testing hypotheses in solid tumors (Ozik et al. 2018). CompuCell3D is a comprehensive modeling platform built by extending the Cellular Potts framework and is capable of capturing complex cell morphologies (Swat et al. 2012). The Hybrid Automata Library (HAL) is a mathematical oncology framework that focuses on layering ABMs with ODEs and PDEs (Bravo et al. 2020). Morpheus provides a powerful and flexible model framework (Starruss et al. 2014), and typically represents cell-based ABMs as either center- or vertex-based. There are many other ready-made frameworks with various advantages and disadvantages, many of which were neatly outlined by the HAL developers (Bravo et al. 2020).

Published cancer and granuloma models have investigated multiple aspects of cancer and TB progression (Metzcar et al. 2019; Norton et al. 2019). These models address important questions around immune dynamics (Castiglione et al. 2005; Lollini et al. 2006; Pennisi et al. 2010; Palazon et al. 2011; Pappalardo et al. 2011; Woelke et al. 2011; Kim et al. 2012; von Eichborn et al. 2013; Pourhasanzade et al. 2017), growth of metastases (Enderling et al. 2009a, b; Biava et al. 2011; Enderling et al. 2012; Wynn et al. 2012), drug resistance (Silva et al. 2010; Powathil et al. 2012; Wang et al. 2015), tumor immunotherapy, tumor-enhancing immune/stromal cells, tumor heterogeneity (Norton et al. 2014), angiogenesis, and more (Poleszczuk et al. 2016; Metzcar et al. 2019; Norton et al. 2019). Gong et al. (2017) developed a multiscale, three-dimensional (3D) ABM of interactions between immune and cancer cells, which revealed emergent global behaviors during tumor development and therapy. Menezes et al. and Calopiz et al. created ABMs detailing the pharmacokinetics of antibody drug conjugate treatment of solid tumors, relating drug penetration to overall impact on treatment efficacy for established tumors (Menezes et al. 2022; Calopiz et al. 2024). A recent study presented a detailed model of nutrient transport through avascular tumors and its impact on tumor growth (Almudarra et al. 2024). Similarly, ABMs have been used to study TB. Warrender et al. used an ABM framework to investigate early Mtb infection (Warrender et al. 2006). More recently, 3-D ABMs have been used to simulate in vitro granuloma models, with a focus on T-cell/Macrophage interactions on granuloma outcomes (Petrucciani et al. 2024). A larger-scale ABM, the "bubble model", was used to study how multiple confluent TB granulomas merge within lungs (Prats et al. 2016).

We have chosen to build on *GranSim*, the C++-based ABM framework that we have created and curated for over 20 years for capturing TB granulomas. We have

previously used *GranSim* to study immune and bacterial dynamics during infection (Cardona et al. 2001, 2005; Marino et al. 2004; Segovia-Juarez et al. 2004; Gammack et al. 2005; Ray et al. 2009), antibiotic treatment (Cilfone et al. 2015a, b; Pienaar et al. 2015a, b; Cicchese et al. 2020a, b; Budak et al. 2023, 2024), perform virtual clinical trials to predict optimal treatment strategies (Marino et al. 2007, 2014; Fallahi-Sichani et al. 2012; Cilfone et al. 2015a, b; Pienaar et al. 2015a, b; Cicchese et al. 2020a, b; Budak et al. 2023, 2024), also incorporating drug resistance (Pienaar et al. 2018). As SCLC tumors share many fundamental components, we create *TumorSim* on our foundational *GranSim* computational architecture platform. Here, we create novel agents, rules and features (Hypoxia inducible factor 1-α (HIF1α), oxygen, interferon gamma (IFN-ɣ), cancer cells etc.) and use wide ranges of parameters to explore a range of tumor model outputs. *TumorSim* reproduces temporal dynamics of cytotoxic T cells and cancer cells during tumor progression, as well as spatial distributions of these cells. A comparison and contrast between mechanisms included in *GranSim* and *TumorSim* is shown in Table 1 showing both overlap and distinction between features.

ABMs have the flexibility to be defined in two or three dimensions, and each choice has advantages and disadvantages. We have previously shown that with appropriate scaling, two-dimensional models accurately capture many aspects of lung lesion development if we assume radial symmetry. Accuracy captures concentration distributions (with scaling between 2-D and 3-D datasets if needed (Renardy et al. 2019)), cell counts, and principle mechanisms that are driving of gross outcomes (Marino et al. 2018; Linderman et al. 2010). We found that model predictions that were captured substantially differently between 2-D and 3-D models were the times it takes for specific cognate-conjugate cell pairs to meet and we showed this in a number of different ABM model formulations (Marino et al. 2018). Other models have used a quantitative systems pharmacology module to determine cancer cell proliferation and spatially homogeneous chemokine concentrations in a 3-D ABM for spatial analysis, but at a high computational cost (Ruiz-Martinez et al. 2022). Dimensional considerations must be made based on the purpose of the model under study. We use 2-D frameworks for both *TumorSim* and *GranSim* because: (1) our goal is to determine principal driving mechanisms for gross outcomes and sensitivity analysis requires hundreds of simulations; (2) 3-D ABM computational cost >2 orders of magnitude larger than 2-D; (3) we do not focus on spatially-dependent specific-cell-interaction events like antigen presentation within lymph nodes; and finally (4) most datasets for both granulomas and tumors are taken from 2-D data (e.g., slices of tissues, staining of tissues, etc.). In our previous work, we have shown that scaling immune ABMs from 2-D to 3-D faithfully captures many aspects of the human immune response that they do not track co-localization of specific cell pairs or detailed cell movement/chemotaxis on the grid (Marino et al. 2018; Renardy et al. 2019).

2.1 *TumorSim*

To simulate emergence of a SCLC tumor, we create *TumorSim*, which captures key cells known to drive basic SCLC immunobiology. We build *TumorSim* as a multi-scale, agent-based model that simulates interactions between immune cells, relevant

Table 1 Comparison and contrast between *GranSim* and *TumorSim* mechanisms

	GranSim	*TumorSim*
Initialization	- Resting macrophages and vascular sources randomly distributed on simulation grid - One macrophage infected with one mycobacterium at the center of the simulation grid	- Vascular sources randomly distributed on simulation grid - A circular neoplasm of ten cancer cell diameter at the center of the simulation grid - Few, and M1 macrophages at the center of the simulation grid
Macrophages	- Present as resting (Mr), activated (Ma), infected (Mi), chronically infected (Mci) - Ma kills Mtb effectively - Mi provides a permissive niche for Mtb to grow - Mci cannot kill Mtb and bursts	- Present as M1 and M2 - M1 kills cancer cells - M2 deactivates CTL - IFN-ɣ polarizes M2 toward M1 phenotype - HIF1α polarizes M1 toward M2 phenotype
T cells	- Present as cytotoxic (CTL), IFN-ɣ -secreting (Tgam) and regulatory (Treg) - CTL and Tgam are proinflammatory and induce apoptosis in Mi and Mci - Treg is anti-inflammatory and downregulate CTL and Tgam	- Present as Treg and CTL - CTL is proinflammatory and kills cancer cells, can be PD-1+ or PD-1- - Treg is anti-inflammatory and deactivates CTLs
Vascular blockage	- Vascular sources blocked depending on the amount of necrotization and cell density	- Dynamic vascular permeability based on the level of hypoxia
Chemokine-cytokine secretion	- Chemokines: CCL2, CCL5 and CXCL9 secreted by Mi, Ma and Mci - Cytokines: TNF-α secreted by Tgam and CTL; IFN-ɣ secreted by Tgam; IL-10 secreted by macrophages, Tregs, and nominally by CTLs	- Chemokines: CCL2, CCL5 secreted by cancer cells, and CXCL9 M1 macrophages - Cytokines: IFN-ɣ secreted by M1 and CTL; - HIF1α implicitly secreted by all cells in low-oxygen environments
Recruitment	- Macrophages and T cells recruited from vascular sources based on the levels of CCL2, CCL5, CXCL9, and TNF-α	- Macrophages and T cells recruited from vascular sources based on the levels of CCL2, CCL5, CXCL9
Proliferation	- Bacteria proliferate with different rates based on the bacterial subpopulation - Immune cells do not proliferate	- Cancer cells proliferate - Immune cells may proliferate
Age-related cell death	Immune cells only	No age-related cell death

molecules and cancer leading to formation of SCLC tumors on a 2-D simulation grid representing 6 mm x 6 mm of lung tissue. In this section, we describe key details of our development of *TumorSim*; full details of our model implementation can be found in our Overview, Design concepts, and Details-formatted model description document (Grimm et al. 2020) (Appendix A).

TumorSim contains two mathematically distinct types of agents. First are discrete agents that move or act based on rules (e.g., cell–cell interactions) at a slow timescale ($\Delta T = 10$ minutes). Discrete agents include vascular sources that serve as a source of cellular recruitment and O_2 levels. All other discrete agents are cellular and include cancer cells that may or may not express the PD-L1 "don't-kill-me" ligand, cytotoxic CD8+ T cells (CTLs) that may or may not express PD-1, regulatory T cells (Treg), and pro- and anti-inflammatory (M1 and M2) macrophages. These are the minimal set of immune cells known to be heavily involved in SCLC lung lesions (Kohli et al. 2022; Li et al. 2022).

Second are continuous agents that are secreted, consumed, or diffuse at a fast timescale ($\Delta t = 4$ seconds). Rules governing continuous agents are discretized partial differential equations (PDEs), allowing a slower timescale. Cells secrete or consume molecules, and rule-based cell–cell interactions occur with probabilities described in the following sections. The continuous agents in *TumorSim* include IFN-ɣ representing a pro-inflammatory factor (Dangaj et al. 2019; Han et al. 2023); and CCL2, CCL5, and CXCL9 as chemokines that direct cell migration (Dangaj et al. 2019; Zheng et al. 2021; Kohli et al. 2022). Further, we track O_2 as a separate continuous agent that diffuses through the microenvironment and is consumed by cellular agents. We use O_2 to infer a hypoxia marker, HIF1α that directs cells towards immunosuppressive phenotypes (Fischer et al. 2007; Palazon et al. 2017). We describe rules and equations in detail in the following subsections.

2.1.1 Initialization

Shortly after the initial malignant transformation, nascent tumor cells may be eliminated by the immune system during an *elimination phase* (Schreiber et al. 2011; Vesely et al. 2011). The elimination phase is likely short and known to involve many components that are outside of the scope of this study, including CD4+ T cells and γδ T cells. For this reason, we initiate our virtual SCLC tumor several days after tumor transformation. As our initial state, we represent a small cluster of cancer cells in lung tissue after immune signals from the elimination phase have allowed for macrophages, Tregs, and CTLs to begin to be recruited (Vesely et al. 2011).

TumorSim tumors begin as small circular lesions with a 10-cell diameter placed upon a 6 mm x 6 mm 2D simulation grid. The grid is divided into 20 μm × 20 μm compartments; this size allows one macrophage, T cell, or cancer cell to occupy a grid compartment as in previous cancer ABMs (Menezes et al. 2022; Calopiz et al. 2024). The entire lung grid section is initially populated by tissue densities of D_{CTL} cytotoxic T cells (CTLs), D_{Treg} regulatory T cells (Tregs), and macrophages (D_{M1} for M1 and D_{M2} for M2). Cancer cells are placed in a grid compartment in a circle of diameter d_{Tumor} centered in the middle of the tissue grid. We also randomly distribute vascular sources onto the 2D grid with a density D_{VS}. This is the density we vascularize

Table 2 Initialization parameters

Parameter	Value/Range	Description
d_{Tumor}	10 cancer cells (200 μm)	Initial tumor diameter
D_{CTL}	[0.0005, 0.0008]	Initial density of CTLs
D_{Treg}	[0.0005, 0.0008]	Initial density of Treg
D_{M1}	[0.00003, 0.00005]	Initial density of M1 macrophages
D_{M2}	[0.0007, 0.001]	Initial density of M2 macrophages
D_{VS}	0.0144	Initial density of vascular sources

Ranges for initial densities of immune cells have been inherited from *GranSim*, as both models share initial densities that reflect the immune environment of otherwise-healthy lung tissue

the lung with for *GranSim* simulations, as the lung tissue is the same (Pienaar et al. 2015a, b). Simulations initialize with both CTLs and cancer cells as PD-1- and PD-L1-, respectively, as SCLC is characterized by low levels of these markers (Pietanza et al. 2015). Initial conditions are shown in Table 2.

2.1.2 T Cells, Cancer Cells, and the PD-1/PD-L1 Axis

The levels of cytotoxic and regulatory T cells associated with tumors, as well as their exposure to pro/anti-inflammatory cytokines, are strongly associated with tumor prognosis (Chaudhary et al. 2016; Dangaj et al. 2019; Han et al. 2023). T cells may express the programmed cell death protein 1 (PD-1) as a surface protein, and tumors cells may produce its ligand (PD-L1). This receptor-ligand pair acts as a natural brake to prevent T cells from killing healthy tissue, but PD-L1 expression by cancer cells inhibits the ability of T cells to kill cancer cells (Wu et al. 2019). HIF1α, produced by cells during hypoxia, induces expression of PD-1 and PD-L1 in CTL (Palazon et al. 2017) and cancer cells (Feng et al. 2017), respectively. Conversely, interleukin-12 signaling induces expression of the transcription factor T-bet, which both directly represses PD-1 transcription and promotes IFN-ɣ production (Hodge-Dufour et al. 1998; Afkarian et al. 2002; Yang et al. 2007; Kao et al. 2011; Burke et al. 2019). Similarly, interleukin-2 indirectly regulates the expression of PD-L1 on cancer cells via CTLs, which has been modeled previously in detail (Gong et al. 2017).

In *TumorSim*, we coarse-grain each of the above interactions as events that stochastically occur during each large-scale timestep. We represent CTLs, Tregs, and cancer cells as discrete agents in our simulated tissue grid. Secretion of the continuous agents IFN-ɣ and HIF1α are described in Sects. 2.1.4 and 2.1.4, respectively. CTLs may be in the discrete states (i) activated or inactive, and (ii) PD-1+ or PD-1-; and cancer cells may be PD-L1+ or PD-L1-. Inactive CTLs may become activated with higher IFN-ɣ or when they are adjacent to (i.e. within the Moore neighborhood of) a cancer cell. An activated CTL adjacent to a cancer cell may kill that cancer cell with a probability based on whether the CTL is PD-1± and/or the cancer cell is PD-L1±. Tregs may deactivate adjacent CTLs. CTLs can induce PD-L1 expression in adjacent cancer cells. PD-1+ CTLs can be deactivated by PD-L1+ cancer cells. High levels of IFN-ɣ may

result in the removal of PD-1 from the surface of CTLs. Equations 1–4 and Table 3 parameterize these interactions:

$$p_{TcytActivation}(C_{IFN\gamma}) = \frac{\text{Vmax}_{\text{CTLActivation}} \cdot C_{IFN\gamma}}{C_{IFN\gamma} + \text{C50}_{\text{CTLActivation}}} \quad (1)$$

$$p_{\text{PD-PD+CTLConversion}}(C_{HIF1\alpha}) = \frac{\text{Vmax}_{\text{PD-PD+CTLConversion}} \cdot C_{HIF1\alpha}}{C_{HIF1\alpha} + C50_{\text{PD-PD+CTLConversion}}} \quad (2)$$

Table 3 T-cell parameters

Parameter	Value/Range	Description
$P_{actPD1\text{-}CTLKillingPDL+Tumor}$	*[0.01, 0.1]*†	Probability of activated PD-1- CTL killing adjacent PD-L1+ cancer cells
$P_{actPD1+CTLKillingPDL+Tumor}$	0	Probability of activated PD-1+ CTL killing adjacent PD-L1+ cancer cells
$P_{actPD1\text{-}CTLKillingPDL\text{-}Tumor}$	*[0.1, 1]*†	Probability of activated PD-1- CTL killing adjacent PD-L1- cancer cells
$P_{actPD1+CTLKillingPDL\text{-}Tumor}$	*[0.01, 0.1]*†	Probability of activated PD-1+ CTL killing adjacent PD-L1- cancer cells
$P_{TregDeactCTL}$	*[0.1, 0.9]*	Probability of Treg deactivating adjacent CTL
$P_{CTL_tumorPDL1}$	*[0.01, 1]*†	Probability of CTL inducing PD-L1 expression in adjacent cancer cells
$P_{tumorPDL1deactivatingPD1+CTL}$	*[0.01, 1]*†	Probability of PD-L1+ cancer cell deactivating adjacent active PD-1+ CTL
$P_{CTLActivationByTumor}$	*[0.01, 1]*†	Probability of CTL activation adjacent to a cancer cell
$\text{Vmax}_{\text{CTLActivation}}$	*[0.1, 0.9]*	Max IFN-ɣ-dependent CTL activation probability
$\text{C50}_{\text{CTLActivation}}$	*[0.5, 3]**	Half-saturation molecule count for IFN-ɣ-dependent CTL activation
$\text{Vmax}_{\text{PD-PD+CTLConversion}}$	*[0.01, 1]*†	Max HIF1α-dependent PD-1- → PD-1+ CTL conversion probability
$\text{C50}_{\text{PD-PD+CTLConversion}}$	*[0.5, 0.9]*	Half-saturation relative concentration for PD-1- → PD-1+ HIF1α-dependent CTL conversion
$\text{Vmax}_{\text{PD+PD-CTLConversion}}$	*[0.01, 1]*†	Max IFN-ɣ -dependent PD-1+ → PD-1- CTL conversion probability
$\text{C50}_{\text{PD+PD-CTLConversion}}$	*[0.5, 3]**	Half-saturation relative concentration for PD-1+ → PD-1- IFN-ɣ -dependent CTL conversion
$\text{Vmax}_{\text{PDL-PDL+TumorConversion}}$	*[0.01, 1]*	Max HIF1α-dependent PD-L1- → PD-L1+ cancer cell conversion probability
$\text{C50}_{\text{PDL-PDL+TumorConversion}}$	*[0.5, 0.9]*	Half-saturation relative concentration for PD-L1- → PD-L1+ HIF1α-dependent cancer cell conversion

Ranges in *italics* are broad-range estimates to explore model capability. *We established these exploratory ranges by finding the maximum and minimum IFN-ɣ molecule counts per grid compartment in pilot simulations. †We sample this range using a log-uniform distribution

$$p_{\text{PD+PD-CTLConversion}}(C_{IFN\gamma}) = \frac{\text{Vmax}_{\text{PD+PD-CTLConversion}} \cdot C_{IFN\gamma}}{C_{IFN\gamma} + C50_{\text{PD+PD-CTLConversion}}} \quad (3)$$

$$p_{\text{PDL-PDL+TumorConversion}}(C_{HIF1\alpha}) = \frac{\text{Vmax}_{\text{PDL-PDL+TumorConversion}} \cdot C_{HIF1\alpha}}{C_{HIF1\alpha} + \text{C50}_{\text{PDL-PDL+TumorConversion}}}. \quad (4)$$

2.1.3 Macrophages

Tumor-associated macrophages are a key component of SCLC and their control (Wang et al. 2019; Zheng et al. 2021; Nabet et al. 2024). They can either be pro-inflammatory and help destroy the tumor or be anti-inflammatory and facilitate tumor growth. They also secrete chemokines important to T-cell recruitment (Sect. 2.1.4). We represent proinflammatory (M1) and anti-inflammatory (M2) macrophages that have been shown to affect tumor progression (Biswas et al. 2008). M1 macrophages are able to kill cancer cells when adjacent to a cancer cell and M2 macrophages are able to deactivate adjacent CTLs. M1 can convert to the M2 phenotype in the presence of high HIF1α levels, as products downstream of HIF1α are associated with M2 polarization (Colegio et al. 2014). M2 can be converted to M1 in the presence of high levels of IFN-ɣ (Nathan et al. 1983). Equations 5–6 and Table 4 describe polarization:

$$p_{M2M1conversion}(C_{IFN\gamma}) = \frac{\text{Vmax}_{\text{M2M1conversion}} \cdot C_{IFN\gamma}}{C_{IFN\gamma} + \text{C50}_{\text{M2M1conversion}}} \quad (5)$$

$$p_{M1M2conversion}(C_{HIF1\alpha}) = \frac{\text{Vmax}_{\text{M1M2conversion}} \cdot C_{HIF1\alpha}}{C_{HIF1\alpha} + \text{C50}_{\text{M1M2conversion}}} \quad (6)$$

Table 4 Macrophage parameters

Parameter	Value/Range	Description
$p_{\text{M1killingTumor}}$	*[0.1, 0.9]*	Probability of M1 killing adjacent cancer cell
$p_{\text{M1activatingCTL}}$	*[0.1, 0.9]*	Probability of M1 activating adjacent CTL
$p_{\text{M2deactivatingCTL}}$	*[0.1, 0.9]*	Probability of M2 deactivating adjacent CTL
$\text{Vmax}_{\text{M1M2conversion}}$	*[0.1, 0.9]*	Max HIF1α-dependent M1→M2 conversion probability
$\text{C50}_{\text{M1M2conversion}}$	*[0.1, 0.9]*	Half-saturation parameter for M1→M2 HIF1α-dependent conversion
$\text{Vmax}_{\text{M2M1conversion}}$	*[0.1, 0.9]*	Max IFN-ɣ-dependent M2→M1 conversion probability
$\text{C50}_{\text{M2M1conversion}}$	*[0.5, 3]*	Half-saturation molecule count for M2→M1 IFN-ɣ-dependent conversion

Ranges in *italics* are a broad-range estimate to explore model capability. We established these exploratory ranges by finding the maximum and minimum IFN-ɣ molecule counts per grid compartment in pilot simulations

2.1.4 Chemokine-Cytokine Secretion and Chemotaxis

Critical components of immune control of SCLC tumors include cytokines and chemokines that activate immune cells and guide cells toward the developing tumor (Schreiber et al. 2011; Kohli et al. 2022). In *TumorSim*, we represent both IFN-ɣ and several chemokines as continuous variables (units of #molecules/grid compartment) that diffuse through tissue and are eventually cleared through degradation. Proinflammatory cells (M1 macrophages and CTLs) secrete IFN-ɣ at the fast timestep (4 s). IFN-ɣ secretion from CTLs decreases with higher HIF1α, as downstream products decrease IFN-ɣ secretion from CD8+ T cells (the most common form of CTL) (Fischer et al. 2007). IFN-ɣ secretion by M1 macrophages occurs at a constant rate, though we assume that macrophage production of IFN-ɣ is less than that of CTLs (Han et al. 2023).

We also assume that cancer cells constitutively produce the chemokines CCL2 and CCL5, known to initially recruit monocytes and T cells, respectively. We also assume that IFN-ɣ can induce M1 macrophages to produce CXCL9, another chemokine associated with CTL responses (Guttman et al. 2016; Dangaj et al. 2019; Kohli et al. 2022). Tregs also migrate in response to CXCL9 and CCL5 (Chaudhary et al. 2016; Moreno Ayala et al. 2023). We allow virtual M1 and M2 macrophages to follow CCL2 and CCL5 gradients, though we note this simplification serves to coarse-grain this chemoattraction prior to polarization (Deci et al. 2018). There is evidence that SCLC silences CCL2 (Zheng et al. 2021) and CCL5 (Dangaj et al. 2019), leading to an affected cytotoxic T-cell response that may undermine PD-1/PD-L1 blockade treatment, so we vary production rates of CCL2 and CCL5 to study this further. Table 5 and Eqs. 7–8 characterize these interactions:

$$s_{\mathrm{IFN}\gamma_{\mathrm{CTL}}}(C_{HIF1\alpha}) = \mathrm{Vmax}_{IFN\gamma_{T\mathrm{cyt}}} \cdot \left(\frac{\mathrm{C50}_{\mathrm{IFN}\gamma_{\mathrm{CTL}}}}{C_{HIF1\alpha} + \mathrm{C50}_{\mathrm{IFN}\gamma_{\mathrm{CTL}}}} \right). \tag{7}$$

$$s_{CLXCL9_{M1}}(C_{IFN\gamma}) = \mathrm{Vmax}_{CXCL9} \cdot \left(\frac{C_{IFN\gamma}}{C_{IFN\gamma} + \mathrm{C50}_{\mathrm{CXCL9}}} \right). \tag{8}$$

2.1.5 Proliferation

SCLC cancer cells are characterized by rampant proliferation (Sen et al. 2025). In *TumorSim*, cancer cells proliferate based on a proliferation time parameter, which determines the time interval needed between two consecutive proliferation events (Table 6). Doubling times for several rapidly-dividing cancer cell types such as glioblastoma and HeLa are between 18–33 h in vitro (Newton et al. 1959; Oraiopoulou et al. 2017). However, doubling times for SCLC tumors have been measured to be between 25 and 217 days, albeit many such measurements are made by the time the tumors are at the cm-scale (Harris et al. 2012). We assume that in vivo conditions will prolong doubling time and investigate virtual SCLC cancer cells with doubling times of 36–48 h. Additionally, some immune cells are known to proliferate in response to cancerous tumor microenvironments (Hombach et al. 2007; Yoon et al. 2010; Blessin

Table 5 IFN-ɣ and chemokine parameters

Parameter	Value/Range	Description
$Vmax_{IFN\gamma_CTL}$	*[0.1, 1]* (1/s)	Max IFN-ɣ secretion rate from cytotoxic T cells
$C50_{IFN\gamma_CTL}$	*[0.1, 0.9]*	Half-saturation parameter for HIF1α-dependent IFN-ɣ secretion rate
$s_{IFN\gamma_M1}$	*[0, 0.01]* (1/s)	IFN-ɣ secretion rate from M1 macrophages
$D_{IFN\gamma}$	1.4e−8 (cm^2/s)	Diffusion coefficient of IFN-ɣ
$\mu_{IFN\gamma}$	0.0158* (1/s)	Clearance rate of IFN-ɣ
$Vmax_{CXCL9}$	12* (1/s)	Maximum secretion rate of CXCL9 by M1 macrophages
$C50_{CXCL9}$	90	Half-saturation molecule count for IFN-ɣ-dependent CXCL9 secretion rate by M1 macrophages
s_{CCL2}	*[0,0.1]* (1/s)	Rate of CCL2 secretion by cancer cells
s_{CCL5}	*[0,0.1]* (1/s)	Rate of CCL5 secretion by cancer cells
D_{CK}	5.2e−08 (cm^2/s)	Diffusion coefficient of CCL2, CCL5, and CXCL9
μ_{CK}	0.00158* (1/s)	Clearance rate of CCL2, CCL5, and CXCL9

Ranges in *italics* are broad-range estimates to explore model capability. *Value adapted from *GranSim*

Table 6 Simulated cell cycle durations and frequency of proliferating phenotype by cell type

Parameter	Value/Range	Description
r_{tumor}	[1.5, 2] days	Cancer cell doubling time
p_{tumor}	[0.65, 1]	Probability that cancer cells are proliferating Ishibashi et al. (2017)
r_{Treg}	5 days	Treg proliferation interval Hombach et al. (2007)
p_{Treg}	0.03	Probability that Tregs are proliferating Blessin et al. (2021)
r_{CTL_rest}	7.5 days	Inactivated CTL proliferation interval Yoon et al. (2010)
p_{CTL_rest}	0.01	Probability that resting CTLs are proliferating Blessin et al. (2021)
r_{CTL_act}	8 h	Activated CTL proliferation interval Yoon et al. (2010), Kretschmer et al. (2023)
p_{CTL_act}	0.05	Probability that active CTLs are proliferating Blessin et al. (2021)
r_{M1}	1.5 days	M1 macrophage proliferation interval *
r_{M2}	2 days	M2 macrophage proliferation interval *
p_M	[0.05, 0.1]	Probability that M1 or M2 macrophages are proliferating *

We estimated cell cycle lengths from the references cited, though true cell cycle durations are dynamically based on many factors that lie beyond the scope of this simulation. Values marked with * are an ansatz, as we could not find specific replication rates in the literature; however, macrophage replication in tumors has been reported (Filiberti et al. 2022)

et al. 2021). We allowed a fraction of immune cells to proliferate based on activation state with cell cycle lengths estimated from literature (as referenced in Table 6). Notably, CTLs are known to have cell cycle durations as short as 2 h that slow substantially after several division rounds (Yoon et al. 2010; Kretschmer et al. 2023); we choose an 8-h cell cycle time to account for this eventual slowing. Table 6 characterizes *TumorSim* proliferation.

2.1.6 Recruitment

Chemokines associated with inflammation and hypoxia recruit immune cells to the tumor microenvironment (Kohli et al. 2022). In *TumorSim*, each vascular source has a probability to recruit immune cells based on levels of local chemokines. The chemokines influencing these probabilities are based on identical reasoning to the chemotaxis model (Deci et al. 2018; Kohli et al. 2022). We assume that both M1 and M2 macrophages are recruited by CCL2 and CCL5, Tregs are recruited by CCL5, and CTLs are recruited by both CCL5 and CXCL9. Newly-recruited CTLs are activated, as we assume activation within lymph nodes occurs prior to their arrival in the tumor microenvironment (Iwai et al. 2021). Table 7 and Eqs. 9–11 characterize recruitment:

$$p_{rec_{M1}}(C_{CCL2},\ C_{CCL5}) = p_{rec_{M2}}(C_{CCL2},\ C_{CCL5}) = b \cdot \frac{\mathrm{Rmax}_M}{2}\left(\frac{C_{CCL2}}{C_{CCL2}+C50_M} + \frac{C_{CCL5}}{C_{CCL5}+C50_M}\right) \quad (9)$$

$$p_{rec_{T_{cyt}}}(C_{CCL5},\ C_{CXCL9}) = b \cdot \frac{\mathrm{Rmax}_{\mathrm{CTL}}}{2}\left(\frac{C_{CCL5}}{C_{CCL5}+\mathrm{C50}_{\mathrm{CTL}}} + \frac{C_{CXCL9}}{C_{CXCL9}+2\cdot\mathrm{C50}_{\mathrm{CTL}}}\right) \quad (10)$$

$$p_{rec_{Treg}}(C_{CCL5}) = b \cdot \mathrm{Rmax}_{\mathrm{Treg}}\frac{C_{CCL5}}{C_{CCL5}+\mathrm{C50}_{\mathrm{Treg}}} \quad (11)$$

where b is the blockage term $Blockage(C_{HIF1\alpha})$ discussed in the next section. The factor of 1/2 in Eqs. 9–10 ensures that each chemokine contributes at most half of the

Table 7 Recruitment parameters

Parameter	Value/Range	Description
$\mathrm{Rmax}_{\mathrm{M}}$	[0.0058, 0.025]	Max recruitment probability of M1 and M2
$\mathrm{Rmax}_{\mathrm{CTL}}$	[0.012, 0.063]	Max recruitment probability of CTL
$\mathrm{Rmax}_{\mathrm{Treg}}$	[0.0094, 0.041]	Max recruitment probability of Treg
$\mathrm{C50}_{\mathrm{M}}$	[2.37, 4.62]	Half-saturation molecule count for M1 and M2 chemokine-dependent recruitment
$\mathrm{C50}_{\mathrm{CTL}}$	[4.76, 10.27]	Half-saturation molecule count for CTL chemokine-dependent recruitment
$\mathrm{C50}_{\mathrm{Treg}}$	[0.94, 2.0]	Half-saturation molecule count for Treg chemokine-dependent recruitment

Ranges are broad-range estimates to explore model capability

maximal recruitment rate, so the total recruitment probability saturates at Rmax when both chemokines are at high concentration. For CTL recruitment (Eq. 10), the half-saturation for CXCL9 is doubled relative to CCL5. Recruitment at each vascular source is competitive: at most one immune cell type is recruited per source per timestep.

2.1.7 Vascular Permeability Modeling

Hypoxia, which frequently accompanies solid tumor development, results in vascular blockage that inhibits the ability of a vascular source to supply immune cells to the tumor microenvironment. In *TumorSim*, we model vascular permeability by calculating the blockage for each vascular source, which depends on levels of hypoxia at the source's location (Economopoulou et al. 2009). To assess the level of hypoxia, we calculate O_2 concentration at steady state within the whole grid using the heat equation and periodic boundary conditions after we initialize an n-by-n grid with the cancer cells, immune cells and vascular sources as

$$\left(\frac{D_{O2}}{\Delta x^2}A - \lambda I\right)u = f \tag{12}$$

where D_{O2} is the diffusion coefficient of O2, Δx is the length of one grid compartment, A is an n^2-by- n^2 Laplacian matrix for periodic boundary conditions, u is an n^2-by-1 vector of O2 concentrations at the simulation grid and f is the n^2-by-1 / vector for the O2 contribution from sources and sinks (see Table 8 parameter descriptions and values). We define the forcing vector f per grid compartment i as:

$$f_i = \begin{cases} -\lambda \cdot O2_{grid} & \text{if the grid } i \text{ does not have any sources or sinks} \\ -\lambda \cdot O2_{grid} - fO2_{VS} \cdot Blockage(C_{HIF1\alpha}) & \text{if grid } i \text{ has a vascular source} \\ -\lambda \cdot O2_{grid} + cO2_j & \text{if grid } i \text{ has a cell type that consumes O2} \end{cases} \tag{13}$$

where oxygen consuming cells are Cancer cells, CTLs, Tregs, M1 macrophages, and M2 macrophages, and $Blockage(C_{HIF1\alpha})$ is defined below (Supplementary Material S1 for additional detail).

Hypoxia induces expression of HIF1α (Li et al. 2022). We model relative HIF1α concentration based on steady state O2 concentrations. Relative HIF1α concentration $C_{HIF1\alpha}$ is a unitless per-grid-compartment value between 0 and 1 that increases with hypoxia (i.e., lower O2 levels), and computed using the following equation (parameterized in Table 8):

$$C_{HIF1\alpha}(O2) = 1 - \frac{O2^{h_{O2}}}{O2^{h_{O2}} + b_{O2}{}^{h_{O2}}} \tag{14}$$

We model vascular blockage based on relative HIF1α (Eq. 14, Table 8 for parameterization). We assume vascular sources that are exposed to higher HIF1α are increasingly blocked as higher HIF1α is associated with leaky vascularization via VEGF (Zhan et al.

Table 8 Vascular permeability, O_2, and HIF1α, and parameters

Parameter	Value/Range	Description
D_{O2}	3.08e−5 (cm^2/s)	Diffusion coefficient of O_2
Δx	20 (μm)	Length of one grid compartment
λ*	0.3 (1/s)	Absorption rate constant
$cO2_{Tumor}$*	6.7e7 (1/s)	Number of O_2 molecules consumed by cancer cells per second
$cO2_{CTL}$*	2.4e6 (1/s)	Number of O_2 molecules consumed by CTL per second
$cO2_{Treg}$*	2.4e6 (1/s)	Number of O_2 molecules consumed by Treg per second
$cO2_{M1}$*	[3.85e7, 6.7e7] (1/s)	Number of O_2 molecules consumed by M1 per second
$cO2_{M2}$*	[3.85e7, 6.7e7] (1/s)	Number of O_2 molecules consumed by M2 per second
$fO2_{VS}$*	1.7e11 (1/s)	Number of O_2 molecules coming through vascular sources per second
$O2_{Grid}$*	9.2e8 (1/s)	Number of O_2 molecules diffusing from the inhaled air in the lungs to the lung tissue per microgrid per second
b_{O2}	[30, 50]†	Half-saturation of O_2 mg/L per grid compartment for HIF1α conversion
h_{O2}	*[1, 5]*	O_2 to relative HIF1α concentration conversion parameter
$b_{blockage}$	*[0.1, 0.9]*	HIF1α level associated with 50% vascular blockage
$h_{blockage}$	*[0.5, 5.0]*	HIF1α to vascular blockage conversion parameter

We present further derivation for parameters marked by * in Supplementary Material S1. †This parameter is based on preliminary simulations where approximately 20 mg/L was a common baseline concentration outside of the tumor

2009). The blockage term is between 0 and 1 and is proportional to HIF1α and quantifies the proportion of molecules allowed to pass through each vascular source, where a value of 0 indicates no passage, 0.5 represents 50% passage, etc. (see f_i). Blockage is calculated as:

$$Blockage(C_{HIF1\alpha}) = \frac{{C_{HIF1\alpha}}^{h_{blockage}}}{{C_{HIF1\alpha}}^{h_{blockage}} + {b_{blockage}}^{h_{blockage}}} \tag{15}$$

2.2 *GranSim*

The immune cellular compositions of lung tumors and granulomas are similar (Fang et al. 2025). To compare whether the most influential mechanisms underpinning them

are also analogous, we present a brief summary of the components of *GranSim*, which captures key cell types that lead to emergent TB granuloma formation and maintenance. These interactions lead to the emergence of a single lung granuloma that is structurally and functionally representative of non-human primate granulomas, the animal TB model closest to human TB disease and also closely resembles human granulomas (Cardona et al. 2001, 2005; Marino et al. 2004; Segovia-Juarez et al. 2004; Gammack et al. 2005; Ray et al. 2009).

GranSim is a multiscale ABM simulating the interactions between immune cells and bacteria (Mtb) on a 2-D simulation grid representing a 6 mm x 6 mm lung tissue. *GranSim* uses discrete and continuous agents using slow and fast timescales ($\Delta T = 10$ minutes and $\Delta t = 6$ seconds, respectively). Discrete *GranSim* agents include cytotoxic, IFN-γ secreting and regulatory T cells; macrophages, Mtb, and vascular sources that serve as loci for cellular recruitment. The grid is divided into 20 μm × 20 μm compartments, we admit a single compartment to contain one macrophage, two T cells, or one macrophage and one T cell. Continuous agents include chemokines (CCL2, CCL5 and CXCL9) and cytokines (TNF-α and IFN-γ, IL-10). Continuous agents are implemented as PDEs, and are updated using an FFT-based PDE solver as in our previous work (Cilfone et al. 2014).

Below is an overview of the major components of *GranSim*. For details and parameter values, see our online documentation at http://malthus.micro.med.umich.edu/GranSim/docs/gransimrules-v2.pdf.

2.2.1 Initialization

TB can be caused by inhaling a single bacterium (Martin et al. 2017). As such, we begin with a single macrophage infected with Mtb at the center of the simulation grid. Resting macrophages and vascular sources are randomly distributed onto the 2-D simulation grid, representing otherwise-healthy tissue. We have both slow-timescale (cellular) and fast-timescale (molecular) mechanisms.

2.2.2 Macrophages

Macrophages provide both the main replicative niche for Mtb and once activated, a primary source of bactericidal activity (Ramakrishnan 2012). Macrophages in *GranSim* assume one of four states depending on their activation and infection statuses: resting, activated, infected and chronically infected. Macrophages are in the 'resting state' when they are first recruited into the simulation grid. They switch into an 'activated state' when they are activated by STAT1 and NFKB-dependent mechanisms and can kill Mtb effectively. They get infected with a defined probability when they are adjacent to Mtb and switch into an 'infected state'. Infected macrophages provide a permissive niche for Mtb that grow within macrophages. Once the number of Mtb within a macrophage reaches a predefined threshold, then the macrophage switches from the 'infected state' into the 'chronically infected state', where it cannot clear the Mtb or move due to highly infected status. Once the number of intracellular Mtb reaches the carrying capacity, the chronically infected macrophage bursts and dies.

2.2.3 T Cells

Mtb-specific T cells are critical for effective control of Mtb, both through inducing apoptosis of infected macrophages, activation of resting macrophages (allowing them to effectively kill Mtb) (Flynn et al. 2022; Winchell et al. 2023). Tregs cells are immunosuppressive, and their activity is associated with poor granuloma outcomes (Flynn et al. 2022). *GranSim* represents three types of T cells: cytotoxic (CTL), IFN-ɣ-secreting (Tgam), and regulatory (Treg). Cytotoxic T and IFN-ɣ-secreting T cells secrete TNF-α, but only IFN-ɣ-secreting T cells secrete IFN-ɣ. Cytotoxic T cells induce perforin/granulysin-mediated apoptosis, whereas IFN-ɣ -secreting T cells induce Fas/FasL mediated apoptosis in infected and chronically infected macrophages. Both mechanisms of apoptosis result in the death of the macrophage along with a portion of their intracellular Mtb. When adjacent, regulatory T cells can downregulate cytotoxic and IFN-ɣ -secreting T cells, which leads to the loss of their cytokine-secreting and apoptosis-inducing abilities.

2.2.4 Vascular Blockage Modeling

As cells in TB granulomas die, dead cellular debris accumulates into a necrotic core (caseum) that serves as a niche for bacterial survival but they cannot replicate; vascular sources are abnormal in caseum, leading to a hypoxic microenvironment (Datta et al. 2015). We model vascular blockage depending on the amount of necrotic tissue (i.e., caseum) and cell density at the vascular source's location. The blockage increases with higher necrotization and higher density. We model the level of necrotization as the ratio of the number of dead cells on that location to a maximum of dead cells allowed in each grid. Once the number of dead cells reaches the maximum value allowed, then we consider the grid as caseated, which means that the vascular source at that location is completely blocked, and cells can no longer move to that location.

2.2.5 Mtb and Bacterial Proliferation

Mtb replicate based on their metabolic state, which differs based on their main niches: within-macrophages (intracellular Mtb), in the interstitial space between live cells (extracellular-replicating), and within caseum (extracellular-nonreplicating) (Ramakrishnan 2012). Each Mtb agent in *GranSim* is assigned a metabolic mode based on their location: intracellular Mtb within macrophages, extracellular Mtb in the cellular region of granulomas and nonreplicating Mtb trapped in the caseum. Intra- and extracellular Mtb proliferate in *GranSim*, but immune cells and nonreplicating Mtb do not proliferate. The total rate of proliferation of intracellular Mtb depends on the adaptive immune response and decreases when adaptive immunity is effective. The rate of proliferation of extracellular Mtb depends on the caseation level and the number of Mtb within a grid compartment, with replication rate decreasing with increased caseation and Mtb burden.

2.2.6 Chemokine-Cytokine Secretion

Similar to tumors, chemokines and cytokines are secreted within granulomas to activate, suppress, or chemoattract cells (Ramakrishnan 2012). In *GranSim*, activated, infected and chronically infected macrophages secrete the chemokines CCL2, CCL5 and CXCL9. Unless they are downregulated by Tregs, CTLs and Tgams are able to secrete cytokines—both CTLs and Tgams secrete TNF-α, while only Tgams cells secrete IFN-ɣ. Macrophages respond to the chemoattraction of CCL2 and CCL5, CTLs to CCL5 and CXCL9, Tregs along CCL5, and Tgam along all CCL2, CCL5, CXCL9.

2.2.7 Recruitment

Cytokines also inform the rate of recruitment of immune cells to the site of Mtb infection (Flynn et al. 2022). We recruit macrophages and T cells from vascular sources. The recruitment rates at each vascular source are dependent upon the concentrations of CCL2, CCL5, CXCL9, and TNF-α in the specified grid compartment similar to the description for *TumorSim*.

2.2.8 Age-Related Cell Death

As granulomas can persist for years (Lin et al. 2018), we allow simulated cells to age and eventually die. During initialization and recruitment, the age of immune cells is randomly sampled between zero and their maximum age. Immune cells die when they reach their corresponding maximum ages.

2.3 Granuloma and Tumor Simulations

Though both *GranSim* and *TumorSim* share many immune components, the underlying biology suggests very different simulation endpoints. Unlike the immune-controlled growth of granulomas, aggressively-growing SCLC tumors continue to expand, often exceeding 3 cm in diameter (Wang et al. 2022). We expect that a virtual SCLC tumor without any immune resistance may exceed a 5 mm x 5 mm region within 15–30 days and overflow our simulated domain; for this reason, we simulate 2 weeks of tumor growth early after the tumor is established. By contrast, we simulate TB granulomas for 300 days to capture both early formation and late-stage maintenance.

To accurately understand how model outcomes depend on parameter values, we ensure that the simulations arising from our parameter ranges well-represent the underlying biology. To ensure a thorough exploration of parameter space, we employ the Latin hypercube sampling (LHS) method (Marino et al. 2008) that creates a stratified random sampling of a given parameter space (Marino et al. 2008; Renardy et al. 2021). For *TumorSim*, we generate 500 parameter sets using the parameter ranges described in Tables 2–8. For *GranSim*, we sample 500 parameter sets using parameter ranges calibrated in our previous work (Budak et al. 2023, 2024). To address stochasticity inherent to the ABM (i.e., aleatory uncertainty) in both *TumorSim* and *GranSim*, we

perform 3 replicate simulations for each parameter sample for a total of 1500 virtual SCLC tumors and 1500 virtual granulomas.

2.4 Classifying Granuloma and Tumor Outcomes

Several common terms have been used to describe tumor status. Uncontrolled proliferation of cancer cells within tumors is frequently described as tumor progression (Schreiber et al. 2011; Li et al. 2022; Kim et al. 2025). Lack of progression is typically characterized by progression-free survival of the patient. Tumor regression is clinically defined as the disappearance of a tumor (Horino et al. 2006). Tumors that neither progress nor regress are called dormant, whether that is due to a balance of pro- and anti-tumor effects, or a consequence of quiescent cells (Li et al. 2015). The vast majority of SCLC tumors progress, with few cases of regression ever reported (Everson 1964; Horino et al. 2006).

In *TumorSim*, we use simulated tumor volume to categorize simulated tumors into three analogous qualitative categories: progressing, dormant, or regressing. We compute tumor volume by counting the number of tumor-associated cells within the simulation. We then infer tumor radius by approximating the tumor area as a circle and estimating tumor volume by assuming a spherical tumor. We describe simulated tumors as progressing if volume increases near-exponentially, dormant if tumor volume plateaus, and regressing if the volume decreases or if all cancer cells die. Supplementary Material S2 shows examples of raw simulation output and tumor outcomes over time, including tumor volume and the sizes of several cell subpopulations.

Similarly, common terms exist to describe TB granulomas. However, granuloma volume is driven by leukocyte count and the bulk of caseous necrosis, fibrosis, and calcification; macroscopic granulomas may be entirely sterile (Lin et al. 2014). Rather, granuloma status is described based on their ability to control Mtb, including sterile, poorly-controlling Mtb, or well-controlling Mtb (although caseum is associated with poor control) (Lin et al. 2014). Poorly-controlling granulomas are associated with the Mtb dissemination, causing disease severity and/or the foundation of new granulomas (Ramakrishnan 2012; Lin et al. 2014, 2018).

In *GranSim*, we use total Mtb count to classify simulated granulomas into one of three states: sterilizing, controlling, and disseminating. Sterilizing granulomas are those that completely clear Mtb within 300 days. Controlling granulomas are those that maintain stable, low levels of Mtb after the adaptive immune system is primed. Disseminating granulomas are those that fail to control Mtb replication, characterized by a continued increase of Mtb throughout the simulation. As with *TumorSim*, in Supplementary Material S2 we show examples of *GranSim* granuloma Mtb count, volumes, and sizes of cell subpopulations over time.

2.5 Uncertainty and Sensitivity Analyses

Complex models like hybrid ABMs are often nonlinear and have hundreds of inputs. Uncertainty and sensitivity analysis allow us to explore parameters that significantly impact outputs of interest. To uncover which dynamics drive heterogeneity in SCLC

tumor and TB granuloma outcomes, we employ the partial rank correlation coefficient (PRCC) method, a robust sensitivity analysis method that quantifies nonlinear monotonic relationships (Marino et al. 2008). Even small PRCC values may indicate significant correlations (Marino et al. 2008), and so we compute p-values associated with each parameter adjusted for multiple comparisons via the Benjamini–Hochberg correction (Gou 2023). We use the PRCC method to analyze the 1500 virtual SCLC tumors and 1500 virtual granulomas generated previously. To ensure that the new *TumorSim* model satisfies the monotonicity requirement of PRCC, we simulated scatterplots showing how *TumorSim* outcomes vary per individual parameters (see Supplementary Material S3).

3 Results

Our goal is to compare and contrast the dynamics of SCLC tumors and TB granulomas using our models *TumorSim* and *GranSim*. One of the key differences between lung cancer and TB granulomas is the duration of disease: SCLC aggressively proliferates and can grow to cm-scale even prior to diagnosis (Wang et al. 2022), whereas many TB granulomas remain < 1 cm even after months (Lin et al. 2014, 2018). To examine drivers of rapid tumor expansion, we have simulated SCLC tumors for 14 days after the initiation of the escape phase. By contrast, we simulate TB granulomas for 300 days to capture a spectrum of long-term controlling and non-controlling granulomas.

3.1 *TumorSim* and *GranSim* Capture Spatiotemporal Features of SCLC Tumors and TB Granulomas

Here, we validate *TumorSim* by comparing gross simulation with reasonable expectations set by published data on lung lesions. In (Fig. 2), we also present side-by-side comparisons between *TumorSim* and *GranSim* outputs to compare and contrast. In Fig. 2A, we present a small lymphocyte-infiltrated SCLC tumor with an effective immune response as observed in human tumors (Chen et al. 2022). Supplementary Fig. S2 separates the agents of this tumor into separate panels. Activated CTLs are located near M1 macrophages and mostly at the tumor boundary as seen in vivo (Yang et al. 2025). We see deactivated CTLs near Tregs within the tumor. Most larger tumors had substantially fewer infiltrating leukocytes, growing essentially unchallenged by immune cells; such tumors are described elsewhere as "cold" and associated with poor outcomes (Galon et al. 2019; Zheng et al. 2021). While the majority of tumors continue to progress (Methods), a small number tend towards dormancy and regression (Fig. 2C). While events of spontaneous SCLC regression are exceedingly rare clinically (Horino et al. 2006), the small size of these simulated tumors ($< \sim 200$ cells) are likely more comparable to the elimination stage of tumor development that cannot be observed in vivo (Schreiber et al. 2011; Vesely et al. 2011). As tumors grow, so do total numbers of overall tumor-associated T cells and macrophages (Fig. 2C–G). By comparison, a majority of simulated TB granulomas are either controlling or sterilizing. Figure 2B shows a representative latent virtual granuloma, where the immune

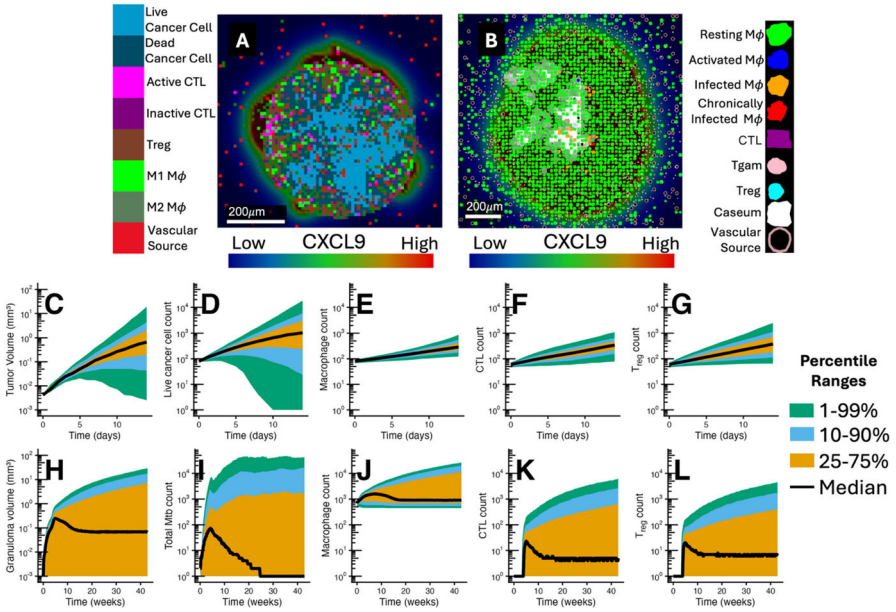


Fig. 2 Spatial and Temporal *GranSim* and *TumorSim* model outputs for comparison and contrast. Both **A** *TumorSim* and **B** *GranSim* simulate spatial interactions of multiple cell types. Both scale bars are 200 microns. **A** A representative *TumorSim* SCLC tumor simulation of a lymphocyte-infiltrated tumor after 14 days of simulation. A mass of cancer cells (blue) is infiltrated by a collection of CTLs and macrophages, while some CTLs are being deactivated by Tregs We show relative levels of CXCL9 as a background heatmap. **B** A representative simulation of a non-sterile granuloma at day 300. Caseum has formed in the center of the infection site and is surrounded by macrophages as well as lymphocytes. We show relative levels of CXCL9 as a background heatmap. **A**–**B** We chose both simulations to demonstrate interaction of multiple cell types. **C**–**L** Each panel shows the median and percentile ranges for multiple temporal outcomes over time for both *TumorSim* **C**–**G** and *GranSim* **H**–**L**. Individual simulation trajectories used to generate these statistics are in Supplementary Fig. S4. Outcomes include lesion volume, Mtb/Cancer cell counts, and leukocyte counts *GranSim* simulations are run for 300 days to capture both early- and late-state dynamics. To plot outcomes on a $\log_{10}$ scale, we have added 1 to all cell counts and 10^{-3}mm^3 to lesion volumes. We simulate *TumorSim* virtual tumors for two weeks due to aggressive growth; we simulate *GranSim* virtual granulomas for 300 days to observe long-term Mtb infection outcomes (color figure online)

system controls but does not completely clear Mtb infection. Supplementary Fig. S3 separates the agents of this granuloma into separate panels. Necrotic caseum accumulates in the center of the Mtb-infected lesion. Overall, we observe an early spike in Mtb count due to the delay in the adaptive immune response, whereafter granuloma volume, Mtb count, macrophage, and T cell count stabilizes for most granulomas (Fig. 2H–L); this reflects the tendency for most granulomas to permit a persistent, latent Mtb infection state (Lin et al. 2018). *GranSim* simulations also capture active TB disease dynamics, as over 40% of our simulated granulomas disseminate, with increasing Mtb counts throughout the simulation (Fig. 2I). In Supplementary Figs. S5–S6, we present storyboard-like progressions of representative simulations for progressing tumors, dormant tumors, and regressing tumors; and non-controlling, controlling, and sterilizing granulomas, respectively. Supplementary Video S1 shows the development

of the tumor in Fig. 2A, and Supplementary Videos S2 and S3 show the development of progressing and regressing tumors, respectively.

3.2 *TumorSim* Captures Distinct Roles of Chemokines During Tumor Development

With the ability to mechanistically simulate 2 large sets of heterogeneous virtual granulomas and tumors, respectively, we analyze each model to determine which parameters (and thereby mechanisms) underpin the heterogeneity of outcomes observed during formation of the lesions. We measure partial rank correlation coefficients (PRCC; see Methods) to capture how parameters that we vary in Tables 2–8 impacted five different tumor-scale outcomes (Fig. 3). Throughout simulations, higher levels of Treg recruitment and faster cancer cell proliferation are associated with larger tumors. Beyond this, we notice a unique separation of early- and late-phase behavior of tumor growth that is driven by distinct mechanisms, occurring near the 1-week timepoint (Fig. 3). Early during tumor growth, macrophage and Treg counts correlate with CCL2 and CCL5 secretion rates in addition to their initial counts. During this time, CCL5 positively correlates with tumor volume—likely due to the recruitment of Tregs. This correlation becomes negative later during tumor growth, around the time that CTL killing of PD-L1+ becomes significantly negatively correlated with tumor volume. This later-phase shift also coincides with the time that CTL levels correlate with CTL activation probability—likely due to the importance of IFN-ɣ production in T-cell recruitment via CXCL9 production by M1 macrophages. While it is well-studied that both CCL5 and CXCL9 perform significant anti-tumor roles (Dangaj et al. 2019; Jin

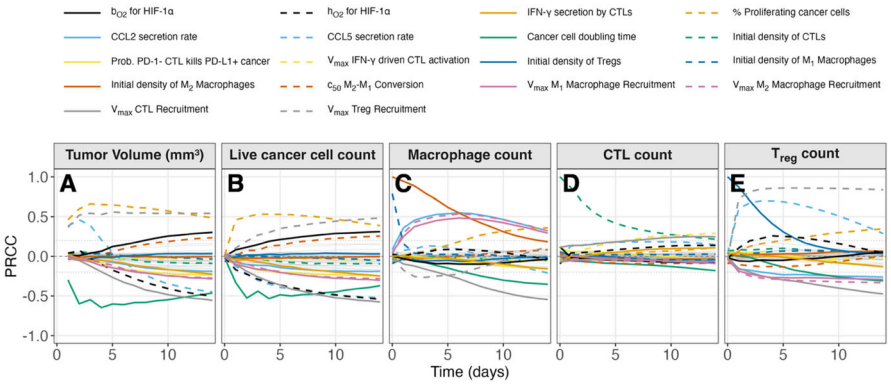


Fig. 3 Parameters influencing *TumorSim* outcomes. To assess mechanisms that influence dynamics and outcomes of *TumorSim*, we present PRCC values over time for every varied *TumorSim* parameter (Methods). We have highlighted PRCC trajectories for those parameters that had significant correlation and |PRCC|> 0.2 for at least one outcome for one or more timepoints ($p < 0.05$ after Benjamini–Hochberg multiple comparison correction (Gou 2023)), while all other PRCC values are shown in gray. PRCC values presented capture the impact of parameters on the model outcomes: **A** tumor volume, **B** live cancer cell count, **C** number of macrophages, **D** CTL count, and **E** Treg count. Some C_{50} values were omitted from presentation for clarity when the associated V_{max}/R_{max} parameters appeared as significant showing similar mechanistic impact (color figure online)

et al. 2024), our simulations suggest that CCL5 may serve a pro-tumor role early during tumor development by recruiting Tregs in the absence of CXCL9. It is during this later stage that PD-1- CTL killing of PD-L1+ cancer cells negatively correlates with tumor volume.

We also observe that macrophage populations negatively correlate with Treg recruitment, likely due to our assuming slower proliferation rates of M2 macrophages. We notice that as simulations progress, all cell populations correlate with faster cancer cell proliferation, likely due to higher net exposure of vascular sources to tumor-associated chemokines. Finally, we observe that as tumors develop, hypoxia-related parameters become more significant, with higher levels of HIF1α correlating with larger tumors, more cancer cells, larger Treg populations, and macrophage counts, likely due to increased CTL PD-1 expression. Lastly, we note that no initial conditions of macrophages or T cells showed as significant to tumor size, suggesting that long-term outcomes are dependent mostly on recruiting effects, which is consistent with development of adaptive immunity.

3.3 Granuloma Outcomes are Determined by a Balance of Pro- and Anti-inflammatory Regulators

From observing spatial and temporal dynamics it is clear there are similarities and differences between behaviors of SCLC and TB systems. To compare, we perform a parallel sensitivity analysis identifying what features control TB lesion outcomes in contrast to SCLC. As above, we apply the PRCC method to assess the impact of each mechanism on five *GranSim* outcomes analogous to *TumorSim* outcomes (Fig. 4). We

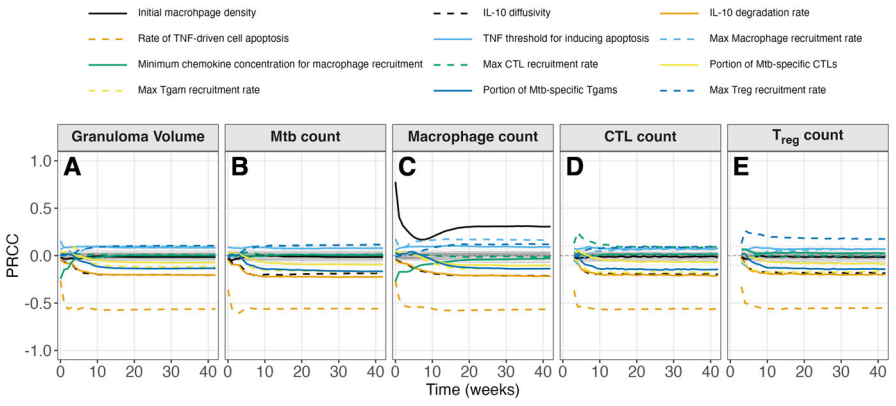


Fig. 4 Parameters influencing *GranSim* outcomes. We present PRCC values over time for every varied *GranSim* parameter for several outcomes. We have highlighted PRCC trajectories for those parameters that had significant correlation for at least one outcome for at one or more timepoints ($p < 0.05$ with Benjamini–Hochberg multiple comparison correction), while all other PRCC values are shown in gray. PRCC values presented capture the impact of parameters on the model outcomes: **A** granuloma volume, **B** total live Mtb count, **C** number of macrophages, **D** CTL count, and **E** Treg count (color figure online)

observe overlapping mechanisms driving bacterial burden and granuloma size, meaning granulomas with higher bacterial burden tend to have larger sizes. Concentration of Interleukin-10 (IL-10), a key anti-inflammatory cytokine, shows significant correlation with larger granulomas and higher levels of Mtb, as observed previously (Cicchese JM et al. 2018). Similarly, lower rates of TNF-α-induced apoptosis, lower recruitment of Tgam, lower cognate Tgam ratio and higher recruitment of macrophages all lead to higher Mtb burden and larger granulomas during the course of infection, consistent with previous experimental and computational studies (Pitt et al. 2012; Cilfone et al. 2013; Cilfone et al. 2015a, b; Lin et al. 2016; Wong et al. 2020). In addition, granuloma size is also sensitive to the thresholds of chemokines needed for macrophage recruitment in the beginning of the infection, such that higher thresholds lead to smaller granulomas due to decreased macrophage recruitment early on. Notably, by around 22 weeks, the drivers of these dynamics settle and we observe no change in drivers of granuloma volume between weeks 22 and 43, despite poorly-controlling granulomas continuing to increase in volume (Fig. 2H).

4 Discussion

Understanding how cell-scale behavior influences macroscopic outcomes is key to understanding the pathology of SCLC and which potential treatments are most promising. Though many mechanisms about SCLC are known, effective treatments remain elusive. In this work we introduce a novel molecule-to-tissue scale model of a lung lesion, *TumorSim*, an agent-based model of SCLC tumors rooted in key cellular and cytokine players to probe which mechanisms principally drive variability in SCLC tumor outcomes.

We base *TumorSim* on the computational framework of *GranSim*, our hybrid ABM representing pulmonary TB granuloma formation (Segovia-Juarez et al. 2004; Ray et al. 2009; Fallahi-Sichani et al. 2011; Cilfone et al. 2013). Lung tumors and TB granulomas share multiple similarities, both in terms of clinical diagnosis (Low et al. 2006; Werutsky et al. 2019) and known drivers of the granuloma/tumor immune microenvironment (Fang et al. 2025). Not surprisingly, data suggest that lung lesions are similar in many immune characteristics and even are mistaken for each other on lung examination (Fang et al. 2025). Implementation of *TumorSim* utilizes similarities and differences describing immune-interaction mechanisms detailed in *GranSim* (Table 1), including our grid-based, lung-tissue simulation environment, molecular- and cell-scale programming of macrophages by T cells in various (anti-)inflammatory states, and an updated oxygen diffusion algorithm. *TumorSim*-specific components include PD-1 and PD-L1 interactions between T cells and cancer cells, descriptions of distinct macrophage states and hypoxia-driven vasculature blockage. We validated *TumorSim* by recapitulating multiple known drivers of tumor outcomes, including the relative interdependence of tumor outcomes on cytotoxic T-cell-to-macrophage interactions via CCL5 and CXCL9 (Dangaj et al. 2019; Jin et al. 2024), as well as the impact of cytotoxic T-cell activity on reduced tumor volume.

Examining *TumorSim* dynamics suggests that tumor dynamics early during tumor escape may be distinct from dynamics driving more mature tumors. Simulations predict that increased CCL5 serves a pro-tumor role during early tumor development by recruiting regulatory T cells before macrophages can mediate recruitment of cytotoxic T cells. During this early phase, Tregs protect the tumor before hypoxia-driven mechanisms become relevant. These could serve as targets for immune boosting treatments of tumors.

We observed several similarities and differences between SCLC tumors and TB granulomas. First, absolute numbers of all cell types—both pro-lesion and anti-lesion—appeared to scale with lesion size. Potent negative regulators (e.g., PD-1/PD-L1 in SCLC; IL-10 in TB; Tregs in both) had consistent impacts on lesion volume and cancer cell/Mtb count. By contrast, TB granulomas are much more effectively limited by the replicative niche of macrophages even when infection is not cleared; whereas non-dormant SCLC lack such constraints and can replicate indefinitely. This is reflected in SCLC proliferation rate correlating with tumor volume, while Mtb replication rate has little correlation with overall granuloma volume or Mtb count.

One goal of this study was to compare and contrast what we learn about both lesion types and their driving mechanisms for intervention purposes. Both *TumorSim* and *GranSim* show improved outcomes with increased cytotoxic activity: tumor volume negatively correlates with CTL and M1 macrophage recruitment (Fig. 3), while granuloma Mtb count negatively correlates with Tgam, CTL, and bactericidal macrophage activity (Fig. 4). Outcomes worsen with the action of regulatory T cells, as Tregs correlate with both increased tumor and granuloma volume. This suggests that targeted inhibition of Treg recruitment or activity could improve both SCLC and TB outcomes. We acknowledge that there is important nuance when considering immune and pharmacological interactions between SCLC and TB treatment. Previous (or present) Mtb infection substantially increases the chance of development of lung cancer (Fang et al. 2025), yet immune checkpoint inhibitor treatment of lung cancer has been associated with reactivation of latent Mtb infection (Anastasopoulou et al. 2019). Still, given the prevalence of TB relapse post-antibiotic treatment (Goletti et al. 2018), it is plausible that many relapse-free TB patients could harbor granulomas after treatment. These granulomas may continue to reshape the lung immune environment via upregulation of local or systemically primed immunosuppressive lymphocytes, possibly resulting in increased Treg involvement during early tumor development.

Interestingly, we noted that in our analysis of *TumorSim*, there was no significant correlation between initial levels of macrophages or T cells and tumor outcomes, suggesting that long-term outcomes are dependent mostly on recruiting effects, which is consistent with development of adaptive immunity. This may not be a true representation as 1) we are only simulating for 14 days and 2) tissue resident memory cells are known to be present in lungs and their role in the elimination phase of SCLC tumor development may contribute to variation in outcomes of people with SCLC or developing lung lesions (Vesely et al. 2011). Advancements in single-cell technology in exploring these early immune interactions may soon allow for more detailed simulations closer to the moment of malignant transformation (Chen et al. 2021).

There are also significant differences between SCLC and TB. SCLC is associated with poor outcomes when more cancer cells proliferate (Ishibashi et al. 2017), which is recapitulated in *TumorSim*. By contrast, Mtb has evolved to replicate more slowly than other bacterial lineages (Menendez et al. 2002; Krupinsky et al. 2025). As expected, this difference is apparent in our PRCC results, given that bacterial replication rate is not a substantial driver of long-term granuloma volume (Fig. 4). Further, the parameters driving *TumorSim* reflect the primary challenge in SCLC clearance is recruitment and engagement of immune cells: most significant PRCC parameters of *TumorSim* focus on recruitment of leukocytes, rather than in-situ activation of those cells. By contrast, many PRCC-significant *GranSim* parameters involve local activation of leukocytes, including cellular sensitivity to TNF-driven apoptosis and the effectiveness of IL-10 signaling. Finally, differences in characteristic timescales means that there are no temporally direct comparisons of driving mechanisms.

TumorSim is a first-generation step toward building a comprehensive model of lung cancer lesions. Though there is a rich and complex body of literature exploring many cell types and cytokines associated with SCLC, it is necessary to simplify the biology for computational tractability. We have represented tumors in 2-D and assume radial symmetry to generate our predictions. While our previous work has shown that many immune mechanisms present in granulomas are well-represented by a 2-D model (Marino et al. 2018; Renardy et al. 2019), this representation may limit some investigations including 3-D tumor shape as well as how immune cells move, find each other, and follow chemokine gradients in actual 3D tissues. Careful consideration would be required to use *TumorSim* to study metastatic processes such as interaction with basement membranes. Studying *TumorSim* in 3-D is an important future direction. Some biologically-distinct cell types have very similar cell–cell interactions at *TumorSim*'s level of biological resolution, e.g., myeloid-derived suppressor cells (MDSCs) and M2 macrophages both are recruited anti-inflammatory cells (Li et al. 2022). The actions of neutrophils and natural killer cells have been included in the action of M1 macrophages and CTLs, respectively. Some cell types are present only in small numbers (e.g., B cells) (Whiteside 2008). Further, some cells are more structural by nature (e.g., fibroblasts (Whiteside 2008)), and are implicitly represented as part of the *TumorSim* grid as background lung tissue. Similarly, several continuous agents have been omitted for similar reasons, e.g., chemokines associated with omitted cell types. Finally, necrosis is a typical feature of SCLC, but is not always found in small samples comparable to those we simulate (Travis 2012). Future versions will explicitly represent these factors and others that are emerging as relevant in SCLC.

The current version of *TumorSim* is exploratory in nature. Many parameter ranges presented in Tables 2–8 have not been calibrated to experimental datasets. In this work, our simulations utilize LHS sampling to generate a stratified sample of parameter ranges allowing for errors in estimating. The sensitivity analyses show the broad impacts of each of the mechanisms on tumor outcomes. In the future, we will integrate more datasets using calibration methods such as CaliPro and Approximate Bayesian Computing with Sequential Monte Carlo sampling to refine these ranges (Joslyn et al. 2021; Nanda et al. 2023). Calibration datasets are surprisingly sparse, as many rates of cellular functions are modified within tumor microenvironments. While the cancer literature is vast, we have found that many cell-scale measurements that could be

used to calibrate models like *TumorSim* have been measured in one kind of cancer but not others and synthesizing a patchwork collection of datasets must be performed carefully. This is left to do with our new collaborations with experimentalists on lung cancers.

The modular structure of our hybrid ABM *TumorSim* will allow us to integrate new biological mechanisms to create more detailed simulations. Further development will allow this platform to be the basis for hypothesis testing and exploring effects of treatment with chemotherapies and host-directed therapies. Detailed simulation of PD-1 blockade will allow us to investigate spatiotemporal effects and cell–cell interactions that underpin heterogeneous treatment responses that clinically define hot versus cold tumors; we may also investigate how this correlates with immune-infiltration based notions of tumor 'heat' (Galon et al. 2019). *TumorSim* may provide valuable insights for treatment of SCLC or other immunologically-similar carcinomas (Sen et al. 2025) which are the subject of our current work.

Supplementary Information The online version contains supplementary material available at https://doi.org/10.1007/s11538-026-01763-8.

Acknowledgements C.T.M. was supported by the Department of Microbiology and Immunology at the UM. This research was supported by the Advanced Cyberinfrastructure Coordination Ecosystem: Services & Support (ACCESS) program through allocations of hours of computer resources # MCB140228. We also thank the Center for Data-Driven Drug Development and Treatment Assessment (DATA; which supported M.B.). We thank Paul Wolberg for computational assistance and support.

Funding Advanced Cyberinfrastructure Coordination Ecosystem: Services & Support (ACCESS),# MCB140228, University of Michigan—Department of Microbiology & Immunology, Center for Data-Driven Drug Development and Treatment Assessment (DATA).

Data Availability All data generated or analyzed during this study are included in this published article and are available upon request to the corresponding authors. Model details for generating simulations in this paper are available in Appendix A and in our on-line supplements. For *TumorSim*, additional information is located at http://malthus.micro.med.umich.edu/TumorSim/ and as an Online Resource. For *GranSim*, additional details and parameter values are available at http://malthus.micro.med.umich.edu/GranSim/docs/gransimrules-v2.pdf.

Declarations

Conflict of interest The authors declare no competing interests.

Open Access This article is licensed under a Creative Commons Attribution 4.0 International License, which permits use, sharing, adaptation, distribution and reproduction in any medium or format, as long as you give appropriate credit to the original author(s) and the source, provide a link to the Creative Commons licence, and indicate if changes were made. The images or other third party material in this article are included in the article's Creative Commons licence, unless indicated otherwise in a credit line to the material. If material is not included in the article's Creative Commons licence and your intended use is not permitted by statutory regulation or exceeds the permitted use, you will need to obtain permission directly from the copyright holder. To view a copy of this licence, visit http://creativecommons.org/licenses/by/4.0/.

References

Afkarian M, Sedy JR, Yang J, Jacobson NG, Cereb N, Yang SY, Murphy TL, Murphy KM (2002) T-bet is a STAT1-induced regulator of IL-12R expression in naive CD4+ T cells. Nat Immunol 3:549–557. https://doi.org/10.1038/ni794

Almudarra MM, Ramírez-Torres A (2024) Examining avascular tumour growth dynamics: a variable-order non-local modelling perspective. Math Mech Solids 30:501–526. https://doi.org/10.1177/10812865241230269

Anastasopoulou A, Ziogas DC, Samarkos M, Kirkwood JM, Gogas H (2019) Reactivation of tuberculosis in cancer patients following administration of immune checkpoint inhibitors: current evidence and clinical practice recommendations. J Immunother Cancer 7:239. https://doi.org/10.1186/s40425-019-0717-7

Ashenafi S, Brighenti S (2022) Reinventing the human tuberculosis (TB) granuloma: learning from the cancer field. Front Immunol 13:1059725. https://doi.org/10.3389/fimmu.2022.1059725

Bayat Mokhtari R, Homayouni TS, Baluch N, Morgatskaya E, Kumar S, Das B, Yeger H (2017) Combination therapy in combating cancer. Oncotarget 8:38022–38043. https://doi.org/10.18632/oncotarget.16723

Biava PM, Basevi M, Biggiero L, Borgonovo A, Borgonovo E, Burigana F (2011) Cancer cell reprogramming: stem cell differentiation stage factors and an agent based model to optimize cancer treatment. Curr Pharm Biotechnol 12:231–242. https://doi.org/10.2174/138920111794295783

Bickett TE, Karam SD (2020) Tuberculosis-cancer parallels in immune response regulation. Int J Mol Sci. https://doi.org/10.3390/ijms21176136

Biswas SK, Sica A, Lewis CE (2008) Plasticity of macrophage function during tumor progression: regulation by distinct molecular mechanisms. J Immunol 180:2011–2017. https://doi.org/10.4049/jimmunol.180.4.2011

Blessin NC, Abu-Hashem R, Mandelkow T, Li W, Simon R, Hube-Magg C, Moller-Koop C, Witt M, Schmidt A, Buscheck F, Fraune C, Luebke AM, Moller K, Jacobsen F, Lutz F, Lennartz M, Steurer S, Sauter G, Hoflmayer D, Tsourlakis MC, Hinsch A, Burandt E, Wilczak W, Minner S, Clauditz TS (2021) Prevalence of proliferating CD8(+) cells in normal lymphatic tissues, inflammation and cancer. Aging (Albany NY) 13:14590–14603. https://doi.org/10.18632/aging.203113

Bonnett LJ, Ken-Dror G, Koh GCKW, Davies GR (2017) Comparing the efficacy of drug regimens for pulmonary tuberculosis: meta-analysis of endpoints in early-phase clinical trials. Clin Infect Dis 65:46–54. https://doi.org/10.1093/cid/cix247

Bravo RR, Baratchart E, West J, Schenck RO, Miller AK, Gallaher J, Gatenbee CD, Basanta D, Robertson-Tessi M, Anderson ARA (2020) Hybrid automata library: a flexible platform for hybrid modeling with real-time visualization. PLoS Comput Biol 16:e1007635. https://doi.org/10.1371/journal.pcbi.1007635

Budak M, Cicchese JM, Maiello P, Borish HJ, White AG, Chishti HB, Tomko J, Frye LJ, Fillmore D, Kracinovsky K, Sakal J, Scanga CA, Lin PL, Dartois V, Linderman JJ, Flynn JL, Kirschner DE (2023) Optimizing tuberculosis treatment efficacy: comparing the standard regimen with Moxifloxacin-containing regimens. PLoS Comput Biol 19:e1010823. https://doi.org/10.1371/journal.pcbi.1010823

Budak M, Via LE, Weiner DM, Barry CE 3rd, Nanda P, Michael G, Mdluli K, Kirschner D (2024) A systematic efficacy analysis of tuberculosis treatment with BPaL-containing regimens using a multiscale modeling approach. CPT Pharmacomet Syst Pharmacol 13:673–685. https://doi.org/10.1002/psp4.13117

Bull JA, Byrne HM (2023) Quantification of spatial and phenotypic heterogeneity in an agent-based model of tumour-macrophage interactions. PLoS Comput Biol 19:e1010994. https://doi.org/10.1371/journal.pcbi.1010994

Burke JD, Young HA (2019) IFN-gamma: a cytokine at the right time, is in the right place. Semin Immunol 43:101280. https://doi.org/10.1016/j.smim.2019.05.002

Calopiz MC, Linderman JJ, Thurber GM (2024) Optimizing solid tumor treatment with antibody-drug conjugates using agent-based modeling: considering the role of a carrier dose and payload class. Pharm Res 41:1109–1120. https://doi.org/10.1007/s11095-024-03715-0

Cardona PJ, Llatjos R, Gordillo S, Diaz J, Vinado B, Ariza A, Ausina V (2001) Towards a 'human-like' model of tuberculosis: intranasal inoculation of LPS induces intragranulomatous lung necrosis in mice infected aerogenically with *Mycobacterium tuberculosis*. Scand J Immunol 53:65–71. https://doi.org/10.1046/j.1365-3083.2001.00842.x

Cardona PJ, Amat I, Gordillo S, Arcos V, Guirado E, Diaz J, Vilaplana C, Tapia G, Ausina V (2005) Immunotherapy with fragmented *Mycobacterium tuberculosis* cells increases the effectiveness of chemotherapy against a chronical infection in a murine model of tuberculosis. Vaccine 23:1393–1398. https://doi.org/10.1016/j.vaccine.2004.09.008

Castiglione F, Toschi F, Bernaschi M, Succi S, Benedetti R, Falini B, Liso A (2005) Computational modeling of the immune response to tumor antigens. J Theor Biol 237:390–400. https://doi.org/10.1016/j.jtbi.2005.04.024

Chaudhary B, Elkord E (2016) Regulatory T cells in the tumor microenvironment and cancer progression: role and therapeutic targeting. Vaccines (Basel). https://doi.org/10.3390/vaccines4030028

Chen WW, Liu W, Li Y, Wang J, Ren Y, Wang G, Chen C, Li H (2021) Deciphering the immune-tumor interplay during early-stage lung cancer development via single-cell technology. Front Oncol 11:716042. https://doi.org/10.3389/fonc.2021.716042

Chen Y, Jin Y, Hu X, Chen M (2022) Infiltrating T lymphocytes in the tumor microenvironment of small cell lung cancer: a state of knowledge review. J Cancer Res Clin Oncol 148:881–895. https://doi.org/10.1007/s00432-021-03895-x

Cicchese J, Sambarey A, Kirschner D, Linderman J, Chandrasekaran S (2020a) A multi-scale pipeline linking drug transcriptomics with pharmacokinetics predicts in vivo interactions of tuberculosis drugs. https://doi.org/10.1101/2020.09.03.281550

Cicchese JM, Dartois V, Kirschner DE, Linderman JJ (2020b) Both pharmacokinetic variability and granuloma heterogeneity impact the ability of the first-line antibiotics to sterilize tuberculosis granulomas. Front Pharmacol 11:333. https://doi.org/10.3389/fphar.2020.00333

Cilfone NA, Perry CR, Kirschner DE, Linderman JJ (2013) Multi-scale modeling predicts a balance of tumor necrosis factor-alpha and interleukin-10 controls the granuloma environment during *Mycobacterium tuberculosis* infection. PLoS ONE 8:e68680. https://doi.org/10.1371/journal.pone.0068680

Cilfone NA, Kirschner DE, Linderman JJ (2014) Strategies for efficient numerical implementation of hybrid multi-scale agent-based models to describe biological systems. Cel Mol Bioeng. https://doi.org/10.1007/s12195-014-0363-6

Cilfone NA, Ford CB, Marino S, Mattila JT, Gideon HP, Flynn JL, Kirschner DE, Linderman JJ (2015a) Computational modeling predicts IL-10 control of lesion sterilization by balancing early host immunity-mediated antimicrobial responses with caseation during *Mycobacterium tuberculosis* infection. J Immunol 194:664–677. https://doi.org/10.4049/jimmunol.1400734

Cilfone NA, Pienaar E, Thurber GM, Kirschner DE, Linderman JJ (2015b) Systems pharmacology approach toward the design of inhaled formulations of rifampicin and isoniazid for treatment of tuberculosis. CPT Pharmacometrics Syst Pharmacol 4:193–203. https://doi.org/10.1002/psp4.22

Cockrell C, An G (2017) Sepsis reconsidered: identifying novel metrics for behavioral landscape characterization with a high-performance computing implementation of an agent-based model. J Theor Biol 430:157–168. https://doi.org/10.1016/j.jtbi.2017.07.016

Colegio OR, Chu NQ, Szabo AL, Chu T, Rhebergen AM, Jairam V, Cyrus N, Brokowski CE, Eisenbarth SC, Phillips GM, Cline GW, Phillips AJ, Medzhitov R (2014) Functional polarization of tumour-associated macrophages by tumour-derived lactic acid. Nature 513:559–563. https://doi.org/10.1038/nature13490

Dangaj D, Bruand M, Grimm AJ, Ronet C, Barras D, Duttagupta PA, Lanitis E, Duraiswamy J, Tanyi JL, Benencia F, Conejo-Garcia J, Ramay HR, Montone KT, Powell DJ Jr., Gimotty PA, Facciabene A, Jackson DG, Weber JS, Rodig SJ, Hodi SF, Kandalaft LE, Irving M, Zhang L, Foukas P, Rusakiewicz S, Delorenzi M, Coukos G (2019) Cooperation between constitutive and inducible chemokines enables T cell engraftment and immune attack in solid tumors. Cancer Cell 35:885-900 e810. https://doi.org/10.1016/j.ccell.2019.05.004

Datta M, Via LE, Kamoun WS, Liu C, Chen W, Seano G, Weiner DM, Schimel D, England K, Martin JD, Gao X, Xu L, Barry CE 3rd, Jain RK (2015) Anti-vascular endothelial growth factor treatment normalizes tuberculosis granuloma vasculature and improves small molecule delivery. Proc Natl Acad Sci U S A. https://doi.org/10.1073/pnas.1424563112

Deci MB, Ferguson SW, Scatigno SL, Nguyen J (2018) Modulating macrophage polarization through CCR2 inhibition and multivalent engagement. Mol Pharm 15:2721–2731. https://doi.org/10.1021/acs.molpharmaceut.8b00237

Dorhoi A, Kotze LA, Berzofsky JA, Sui Y, Gabrilovich DI, Garg A, Hafner R, Khader SA, Schaible UE, Kaufmann SH, Walzl G, Lutz MB, Mahon RN, Ostrand-Rosenberg S, Bishai W, Du Plessis N

(2020) Therapies for tuberculosis and AIDS: myeloid-derived suppressor cells in focus. J Clin Invest 130:2789–2799. https://doi.org/10.1172/JCI136288

Economopoulou M, Langer HF, Celeste A, Orlova VV, Choi EY, Ma M, Vassilopoulos A, Callen E, Deng C, Bassing CH, Boehm M, Nussenzweig A, Chavakis T (2009) Histone H2AX is integral to hypoxia-driven neovascularization. Nat Med 15:553–558. https://doi.org/10.1038/nm.1947

Enderling H, Anderson AR, Chaplain MA, Beheshti A, Hlatky L, Hahnfeldt P (2009a) Paradoxical dependencies of tumor dormancy and progression on basic cell kinetics. Cancer Res 69:8814–8821. https://doi.org/10.1158/0008-5472.CAN-09-2115

Enderling H, Hlatky L, Hahnfeldt P (2009b) Migration rules: tumours are conglomerates of self-metastases. Br J Cancer 100:1917–1925. https://doi.org/10.1038/sj.bjc.6605071

Enderling H, Hlatky L, Hahnfeldt P (2012) The promoting role of a tumour-secreted chemorepellent in self-metastatic tumour progression. Math Med Biol 29:21–29. https://doi.org/10.1093/imammb/dqq015

Everson TC (1964) Spontaneous regression of cancer. Ann N Y Acad Sci 114:721–735. https://doi.org/10.1111/j.1749-6632.1964.tb40991.x

Fabrizio FP (2025) Unlocking lung cancer cell dormancy: an epigenetic perspective. Int J Mol Sci. https://doi.org/10.3390/ijms262210997

Fallahi-Sichani M, El-Kebir M, Marino S, Kirschner DE, Linderman JJ (2011) Multiscale computational modeling reveals a critical role for TNF-alpha receptor 1 dynamics in tuberculosis granuloma formation. J Immunol 186:3472–3483. https://doi.org/10.4049/jimmunol.1003299

Fallahi-Sichani M, Flynn JL, Linderman JJ, Kirschner DE (2012) Differential risk of tuberculosis reactivation among anti-TNF therapies is due to drug binding kinetics and permeability. J Immunol 188:3169–3178. https://doi.org/10.4049/jimmunol.1103298

Fang C, He X, Tang F, Wang Z, Pan C, Zhang Q, Wu J, Wang Q, Liu D, Zhang Y (2025) Where lung cancer and tuberculosis intersect: recent advances. Front Immunol 16:1561719. https://doi.org/10.3389/fimmu.2025.1561719

Feng J, Yang H, Zhang Y, Wei H, Zhu Z, Zhu B, Yang M, Cao W, Wang L, Wu Z (2017) Tumor cell-derived lactate induces TAZ-dependent upregulation of PD-L1 through GPR81 in human lung cancer cells. Oncogene 36:5829–5839. https://doi.org/10.1038/onc.2017.188

Filiberti S, Russo M, Lonardi S, Bugatti M, Vermi W, Tournier C, Giurisato E (2022) Self-renewal of macrophages: tumor-released factors and signaling pathways. Biomedicines. https://doi.org/10.3390/biomedicines10112709

Fischer K, Hoffmann P, Voelkl S, Meidenbauer N, Ammer J, Edinger M, Gottfried E, Schwarz S, Rothe G, Hoves S, Renner K, Timischl B, Mackensen A, Kunz-Schughart L, Andreesen R, Krause SW, Kreutz M (2007) Inhibitory effect of tumor cell-derived lactic acid on human T cells. Blood 109:3812–3819. https://doi.org/10.1182/blood-2006-07-035972

Flynn JL, Chan J (2022) Immune cell interactions in tuberculosis. Cell 185:4682–4702. https://doi.org/10.1016/j.cell.2022.10.025

Galon J, Bruni D (2019) Approaches to treat immune hot, altered and cold tumours with combination immunotherapies. Nat Rev Drug Discov 18:197–218. https://doi.org/10.1038/s41573-018-0007-y

Gammack D, Ganguli S, Marino S, Segovia-Juarez J, Kirschner DE (2005) Understanding the immune response in tuberculosis using different mathematical models and biological scales. Multiscale Model Simul 3:312–345

Ghaffarizadeh A, Heiland R, Friedman SH, Mumenthaler SM, Macklin P (2018) PhysiCell: an open source physics-based cell simulator for 3-D multicellular systems. PLoS Comput Biol 14:e1005991. https://doi.org/10.1371/journal.pcbi.1005991

Global Tuberculosis Report 2025. 1st edn, (World Health Organization, 2025)

Goletti D, Arlehamn CSL, Scriba TJ, Anthony R, Cirillo DM, Alonzi T, Denkinger CM, Cobelens F (2018) Can we predict tuberculosis cure? What tools are available? Eur Respir J. https://doi.org/10.1183/13993003.01089-2018

Gong C, Milberg O, Wang B, Vicini P, Narwal R, Roskos L, Popel AS (2017) A computational multiscale agent-based model for simulating spatio-temporal tumour immune response to PD1 and PDL1 inhibition. J R Soc Interface. https://doi.org/10.1098/rsif.2017.0320

Gou J (2023) On dependence assumption in *p*-value based multiple test procedures. J Biopharm Stat 33:596–610. https://doi.org/10.1080/10543406.2022.2162066

Grimm V, Railsback SF, Vincenot CE, Berger U, Gallagher C, Deangelis DL, Edmonds B, Ge J, Giske J, Groeneveld J, Johnston ASA, Milles A, Nabe-Nielsen J, Polhill JG, Radchuk V, Rohwäder M-S,

Stillman RA, Thiele JC, Ayllón D (2020) The ODD protocol for describing agent-based and other simulation models: a second update to improve clarity, replication, and structural realism. J Artif Soc Soc Simul. https://doi.org/10.18564/jasss.4259

Guttman O, Lewis EC (2016) M2-like macrophages and tumor-associated macrophages: overlapping and distinguishing properties en route to a safe therapeutic potential. Integr Cancer Sci Ther. https://doi.org/10.15761/icst.1000204

Han J, Wu M, Liu Z (2023) Dysregulation in IFN-gamma signaling and response: the barricade to tumor immunotherapy. Front Immunol 14:1190333. https://doi.org/10.3389/fimmu.2023.1190333

Harris K, Khachaturova I, Azab B, Maniatis T, Murukutla S, Chalhoub M, Hatoum H, Kilkenny T, Elsayegh D, Maroun R, Alkaied H (2012) Small cell lung cancer doubling time and its effect on clinical presentation: a concise review. Clin Med Insights Oncol. https://doi.org/10.4137/CMO.S9633

Ho LJ, Yang HY, Chung CH, Chang WC, Yang SS, Sun CA, Chien WC, Su RY (2021) Increased risk of secondary lung cancer in patients with tuberculosis: a nationwide, population-based cohort study. PLoS ONE 16:e0250531. https://doi.org/10.1371/journal.pone.0250531

Hodge-Dufour J, Marino MW, Horton MR, Jungbluth A, Burdick MD, Strieter RM, Noble PW, Hunter CA, Pure E (1998) Inhibition of interferon gamma induced interleukin 12 production: a potential mechanism for the anti-inflammatory activities of tumor necrosis factor. Proc Natl Acad Sci U S A 95:13806–13811. https://doi.org/10.1073/pnas.95.23.13806

Hombach AA, Kofler D, Hombach A, Rappl G, Abken H (2007) Effective proliferation of human regulatory T cells requires a strong costimulatory CD28 signal that cannot be substituted by IL-2. J Immunol 179:7924–7931. https://doi.org/10.4049/jimmunol.179.11.7924

Horino T, Takao T, Yamamoto M, Geshi T, Hashimoto K (2006) Spontaneous remission of small cell lung cancer: a case report and review in the literature. Lung Cancer 53:249–252. https://doi.org/10.1016/j.lungcan.2006.05.011

Ishibashi N, Maebayashi T, Aizawa T, Sakaguchi M, Nishimaki H, Masuda S (2017) Correlation between the Ki-67 proliferation index and response to radiation therapy in small cell lung cancer. Radiat Oncol 12:16. https://doi.org/10.1186/s13014-016-0744-1

Iwai T, Sugimoto M, Patil NS, Bower D, Suzuki M, Kato C, Yorozu K, Kurasawa M, Shames DS, Kondoh O (2021) Both T cell priming in lymph node and CXCR3-dependent migration are the key events for predicting the response of atezolizumab. Sci Rep 11:13912. https://doi.org/10.1038/s41598-021-93113-y

Jin Y, Wu Y, Reuben A, Zhu L, Gay CM, Wu Q, Zhou X, Mo H, Zheng Q, Ren J, Fang Z, Peng T, Wang N, Ma L, Lungevity PIC, Fan Y, Song H, Zhang J, Chen M (2024) Author correction: single-cell and spatial proteo-transcriptomic profiling reveals immune infiltration heterogeneity associated with neuroendocrine features in small cell lung cancer. Cell Discov 10:126. https://doi.org/10.1038/s41421-024-00755-z

Jm C, Evans S, Hult C, Lr J, Wessler T, Ja M, Marino S, Na C, Jt M, Jj L, De K (2018) Dynamic balance of pro- and anti-inflammatory signals controls disease and limits pathology. Immunol Rev 285:147–167

Joslyn LR, Kirschner DE, Linderman JJ (2021) CaliPro: a calibration protocol that utilizes parameter density estimation to explore parameter space and calibrate complex biological models. Cell Mol Bioeng 14:31–47. https://doi.org/10.1007/s12195-020-00650-z

Kao C, Oestreich KJ, Paley MA, Crawford A, Angelosanto JM, Ali MA, Intlekofer AM, Boss JM, Reiner SL, Weinmann AS, Wherry EJ (2011) Transcription factor T-bet represses expression of the inhibitory receptor PD-1 and sustains virus-specific CD8+ T cell responses during chronic infection. Nat Immunol 12:663–671. https://doi.org/10.1038/ni.2046

Kerantzas CA, Jacobs WR Jr. (2017) Origins of combination therapy for tuberculosis: lessons for future antimicrobial development and application. Mbio. https://doi.org/10.1128/mBio.01586-16

Kim PS, Lee PP (2012) Modeling protective anti-tumor immunity via preventative cancer vaccines using a hybrid agent-based and delay differential equation approach. PLoS Comput Biol 8:e1002742. https://doi.org/10.1371/journal.pcbi.1002742

Kim SY, Park HS, Chiang AC (2025) Small cell lung cancer: a review. JAMA 333:1906–1917. https://doi.org/10.1001/jama.2025.0560

Kohli K, Pillarisetty VG, Kim TS (2022) Key chemokines direct migration of immune cells in solid tumors. Cancer Gene Ther 29:10–21. https://doi.org/10.1038/s41417-021-00303-x

Kretschmer L, Fuchs N, Busch DH, Buchholz VR (2023) Picking up speed: cell cycle regulation during effector CD8(+) T cell differentiation. Med Microbiol Immunol 212:253–260. https://doi.org/10.1007/s00430-023-00768-7

Krupinsky KC, Michael CT, Nanda P, Mattila JT, Kirschner D (2025) Distinguishing multiple roles of T cell and macrophage involvement in determining lymph node fates during *Mycobacterium tuberculosis* infection. PLoS Comput Biol 21:e1013033. https://doi.org/10.1371/journal.pcbi.1013033

Lasser SA, Ozbay Kurt FG, Arkhypov I, Utikal J, Umansky V (2024) Myeloid-derived suppressor cells in cancer and cancer therapy. Nat Rev Clin Oncol 21:147–164. https://doi.org/10.1038/s41571-023-00846-y

Li J, Jiang E, Wang X, Shangguan AJ, Zhang L, Yu Z (2015) Dormant cells: the original cause of tumor recurrence and metastasis. Cell Biochem Biophys 72:317–320. https://doi.org/10.1007/s12013-014-0477-4

Li T, Qiao T (2022) Unraveling tumor microenvironment of small-cell lung cancer: implications for immunotherapy. Semin Cancer Biol 86:117–125. https://doi.org/10.1016/j.semcancer.2022.09.005

Lin PL, Ford CB, Coleman MT, Myers AJ, Gawande R, Ioerger T, Sacchettini J, Fortune SM, Flynn JL (2014) Sterilization of granulomas is common in active and latent tuberculosis despite within-host variability in bacterial killing. Nat Med 20:75–79. https://doi.org/10.1038/nm.3412

Lin PL, Maiello P, Gideon HP, Coleman MT, Cadena AM, Rodgers MA, Gregg R, O'malley M, Tomko J, Fillmore D, Frye LJ, Rutledge T, Difazio RM, Janssen C, Klein E, Andersen PL, Fortune SM, Flynn JL (2016) PET CT identifies reactivation risk in cynomolgus macaques with latent M. Tuberculosis. PLoS Pathog 12:e1005739. https://doi.org/10.1371/journal.ppat.1005739

Lin PL, Flynn JL (2018) The end of the binary era: revisiting the spectrum of tuberculosis. J Immunol 201:2541–2548. https://doi.org/10.4049/jimmunol.1800993

Linderman JJ, Riggs T, Pande M, Miller M, Marino S, Kirschner DE (2010) Characterizing the dynamics of CD4+ T cell priming within a lymph node. J Immunol 184:2873–2885. https://doi.org/10.4049/jimmunol.0903117

Liu R, Higley KA, Swat MH, Chaplain MJ, Powathil GG, Glazier JA (2021) Development of a coupled simulation toolkit for computational radiation biology based on Geant4 and CompuCell3D. Phys Med Biol 66:045026. https://doi.org/10.1088/1361-6560/abd4f9

Lollini PL, Motta S, Pappalardo F (2006) Discovery of cancer vaccination protocols with a genetic algorithm driving an agent based simulator. BMC Bioinformatics 7:352. https://doi.org/10.1186/1471-2105-7-352

Low SY, Eng P, Keng GH, Ng DC (2006) Positron emission tomography with CT in the evaluation of non-small cell lung cancer in populations with a high prevalence of tuberculosis. Respirology 11:84–89. https://doi.org/10.1111/j.1440-1843.2006.00789.x

Lowery FJ, Goff SL, Gasmi B, Parkhurst MR, Ratnam NM, Halas HK, Shelton TE, Langhan MM, Bhasin A, Dinerman AJ, Dulemba V, Goldlust IS, Gustafson AM, Hakim AA, Hitscherich KJ, Kenney LM, Levy L, Rault-Wang JG, Bera A, Ray S, Seavey CD, Hoang CD, Hernandez JM, Gartner JJ, Sindiri S, Prickett TD, Mcintyre LS, Krishna S, Robbins PF, Klemen ND, Kwong MLM, Yang JC, Rosenberg SA (2025) Neoantigen-specific tumor-infiltrating lymphocytes in gastrointestinal cancers: a phase 2 trial. Nat Med 31:1994–2003. https://doi.org/10.1038/s41591-025-03627-5

Marino S, Kirschner DE (2004) The human immune response to *Mycobacterium tuberculosis* in lung and lymph node. J Theor Biol 227:463–486

Marino S, Sud D, Plessner H, Lin PL, Chan J, Flynn JL, Kirschner DE (2007) Differences in reactivation of tuberculosis induced from anti-TNF treatments are based on bioavailability in granulomatous tissue. PLoS Comput Biol 3:1909–1924. https://doi.org/10.1371/journal.pcbi.0030194

Marino S, Hogue IB, Ray CJ, Kirschner DE (2008) A methodology for performing global uncertainty and sensitivity analysis in systems biology. J Theor Biol 254:178–196. https://doi.org/10.1016/j.jtbi.2008.04.011

Marino S, Baxter NT, Huffnagle GB, Petrosino JF, Schloss PD (2014) Mathematical modeling of primary succession of murine intestinal microbiota. Proc Natl Acad Sci U S A 111:439–444. https://doi.org/10.1073/pnas.1311322111

Marino S, Hult C, Wolberg P, Linderman JJ, Kirschner DE (2018) The role of dimensionality in understanding granuloma formation. Computation. https://doi.org/10.3390/computation6040058

Martin CJ, Cadena AM, Leung VW, Lin PL, Maiello P, Hicks N, Chase MR, Flynn JL, Fortune SM (2017) Digitally barcoding mycobacterium tuberculosis reveals in vivo infection dynamics in the macaque model of tuberculosis. Mbio. https://doi.org/10.1128/mBio.00312-17

Menendez MC, Garcia MJ, Navarro MC, Gonzalez-Y-Merchand JA, Rivera-Gutierrez S, Garcia-Sanchez L, Cox RA (2002) Characterization of an rRNA operon (rrnB) of *Mycobacterium fortuitum* and other

mycobacterial species: implications for the classification of mycobacteria. J Bacteriol 184:1078–1088. https://doi.org/10.1128/jb.184.4.1078-1088.2002

Menezes B, Khera E, Calopiz M, Smith MD, Ganno ML, Cilliers C, Abu-Yousif AO, Linderman JJ, Thurber GM (2022) Pharmacokinetics and pharmacodynamics of TAK-164 antibody drug conjugate coadministered with unconjugated antibody. AAPS J 24:107. https://doi.org/10.1208/s12248-022-00756-4

Metzcar J, Wang Y, Heiland R, Macklin P (2019) A review of cell-based computational modeling in cancer biology. JCO Clin Cancer Inform 3:1–13. https://doi.org/10.1200/CCI.18.00069

Millar JA, Butler JR, Evans S, Mattila JT, Linderman JJ, Flynn JL, Kirschner DE (2020) Spatial organization and recruitment of non-specific T cells may limit T cell-macrophage interactions within *Mycobacterium tuberculosis* granulomas. Front Immunol 11:613638. https://doi.org/10.3389/fimmu.2020.613638

Mirams GR, Arthurs CJ, Bernabeu MO, Bordas R, Cooper J, Corrias A, Davit Y, Dunn SJ, Fletcher AG, Harvey DG, Marsh ME, Osborne JM, Pathmanathan P, Pitt-Francis J, Southern J, Zemzemi N, Gavaghan DJ (2013) Chaste: an open source C++ library for computational physiology and biology. PLoS Comput Biol 9:e1002970. https://doi.org/10.1371/journal.pcbi.1002970

Mohsin N, Enderling H, Brady-Nicholls R, Zahid MU (2024) Simulating tumor volume dynamics in response to radiotherapy: implications of model selection. J Theor Biol 576:111656. https://doi.org/10.1016/j.jtbi.2023.111656

Moreno Ayala MA, Campbell TF, Zhang C, Dahan N, Bockman A, Prakash V, Feng L, Sher T, Dupage M (2023) CXCR3 expression in regulatory T cells drives interactions with type I dendritic cells in tumors to restrict CD8(+) T cell antitumor immunity. Immunity 56:1613–1630. https://doi.org/10.1016/j.immuni.2023.06.003

Nabet BY, Hamidi H, Lee MC, Banchereau R, Morris S, Adler L, Gayevskiy V, Elhossiny AM, Srivastava MK, Patil NS, Smith KA, Jesudason R, Chan C, Chang PS, Fernandez M, Rost S, Mcginnis LM, Koeppen H, Gay CM, Minna JD, Heymach JV, Chan JM, Rudin CM, Byers LA, Liu SV, Reck M, Shames DS (2024) Immune heterogeneity in small-cell lung cancer and vulnerability to immune checkpoint blockade. Cancer Cell 42:429–443. https://doi.org/10.1016/j.ccell.2024.01.010

Nanda P, Kirschner DE (2023) Calibration methods to fit parameters within complex biological models. Front Appl Math Stat. https://doi.org/10.3389/fams.2023.1256443

Nathan CF, Murray HW, Wiebe ME, Rubin BY (1983) Identification of interferon-gamma as the lymphokine that activates human macrophage oxidative metabolism and antimicrobial activity. J Exp Med 158:670–689. https://doi.org/10.1084/jem.158.3.670

Newton AA, Wildy P (1959) Parasynchronous division of HeLa cells. Exp Cell Res 16:624–635. https://doi.org/10.1016/0014-4827(59)90130-2

Norton KA, Popel AS (2014) An agent-based model of cancer stem cell initiated avascular tumour growth and metastasis: the effect of seeding frequency and location. J R Soc Interface 11:20140640. https://doi.org/10.1098/rsif.2014.0640

Norton KA, Gong C, Jamalian S, Popel AS (2019) Multiscale agent-based and hybrid modeling of the tumor immune microenvironment. Processes (Basel). https://doi.org/10.3390/pr7010037

Oraiopoulou ME, Tzamali E, Tzedakis G, Vakis A, Papamatheakis J, Sakkalis V (2017) In vitro/in silico study on the role of doubling time heterogeneity among primary glioblastoma cell lines. Biomed Res Int 2017:8569328. https://doi.org/10.1155/2017/8569328

Ormerod LP (2005) Multidrug-resistant tuberculosis (MDR-TB): epidemiology, prevention and treatment. Br Med Bull 73–74:17–24. https://doi.org/10.1093/bmb/ldh047

Ozik J, Collier N, Wozniak JM, Macal C, Cockrell C, Friedman SH, Ghaffarizadeh A, Heiland R, An G, Macklin P (2018) High-throughput cancer hypothesis testing with an integrated PhysiCell-EMEWS workflow. BMC Bioinformatics 19:483. https://doi.org/10.1186/s12859-018-2510-x

Palazon A, Teijeira A, Martinez-Forero I, Hervas-Stubbs S, Roncal C, Penuelas I, Dubrot J, Morales-Kastresana A, Perez-Gracia JL, Ochoa MC, Ochoa-Callejero L, Martinez A, Luque A, Dinchuk J, Rouzaut A, Jure-Kunkel M, Melero I (2011) Agonist anti-CD137 mAb act on tumor endothelial cells to enhance recruitment of activated T lymphocytes. Cancer Res 71:801–811. https://doi.org/10.1158/0008-5472.CAN-10-1733

Palazon A, Tyrakis PA, Macias D, Velica P, Rundqvist H, Fitzpatrick S, Vojnovic N, Phan AT, Loman N, Hedenfalk I, Hatschek T, Lovrot J, Foukakis T, Goldrath AW, Bergh J, Johnson RS (2017) An HIF-1alpha/VEGF-A axis in cytotoxic T cells regulates tumor progression. Cancer Cell 32(669–683):e665. https://doi.org/10.1016/j.ccell.2017.10.003

Pappalardo F, Martinez Forero I, Pennisi M, Palazon A, Melero I, Motta S (2011) SimB16: modeling induced immune system response against B16-melanoma. PLoS ONE 6:e26523. https://doi.org/10.1371/journal.pone.0026523

Pennisi M, Pappalardo F, Palladini A, Nicoletti G, Nanni P, Lollini PL, Motta S (2010) Modeling the competition between lung metastases and the immune system using agents. BMC Bioinformatics 11(Suppl 7):S13. https://doi.org/10.1186/1471-2105-11-S7-S13

Peranzoni E, Lemoine J, Vimeux L, Feuillet V, Barrin S, Kantari-Mimoun C, Bercovici N, Guerin M, Biton J, Ouakrim H, Regnier F, Lupo A, Alifano M, Damotte D, Donnadieu E (2018) Macrophages impede CD8 T cells from reaching tumor cells and limit the efficacy of anti-PD-1 treatment. Proc Natl Acad Sci U S A 115:E4041–E4050. https://doi.org/10.1073/pnas.1720948115

Petrucciani A, Hoerter A, Kotze L, Du Plessis N, Pienaar E (2024) Agent-based model predicts that layered structure and 3D movement work synergistically to reduce bacterial load in 3D in vitro models of tuberculosis granuloma. PLoS Comput Biol 20:e1012266. https://doi.org/10.1371/journal.pcbi.1012266

Pienaar E, Cilfone NA, Lin PL, Dartois V, Mattila JT, Butler JR, Flynn JL, Kirschner DE, Linderman JJ (2015a) A computational tool integrating host immunity with antibiotic dynamics to study tuberculosis treatment. J Theor Biol 367:166–179. https://doi.org/10.1016/j.jtbi.2014.11.021

Pienaar E, Dartois V, Linderman JJ, Kirschner DE (2015b) In silico evaluation and exploration of antibiotic tuberculosis treatment regimens. BMC Syst Biol 9:79. https://doi.org/10.1186/s12918-015-0221-8

Pienaar E, Linderman J (2018) Emergence and selection of isoniazid and rifampin resistance in tuberculosis granulomas. PLoS ONE. https://doi.org/10.1371/journal.pone.0196322

Pietanza MC, Byers LA, Minna JD, Rudin CM (2015) Small cell lung cancer: will recent progress lead to improved outcomes? Clin Cancer Res 21:2244–2255. https://doi.org/10.1158/1078-0432.CCR-14-2958

Pitt JM, Stavropoulos E, Redford PS, Beebe AM, Bancroft GJ, Young DB, O'garra A (2012) Blockade of IL-10 signaling during bacillus Calmette-Guerin vaccination enhances and sustains Th1, Th17, and innate lymphoid IFN-gamma and IL-17 responses and increases protection to Mycobacterium tuberculosis infection. J Immunol 189:4079–4087. https://doi.org/10.4049/jimmunol.1201061

Poleszczuk J, Macklin P, Enderling H (2016) Agent-Based Modeling of Cancer Stem Cell Driven Solid Tumor Growth. Methods in molecular biology (Clifton, N.J 1516:335–346. https://doi.org/10.1007/7651_2016_346

Pourhasanzade F, Sabzpoushan SH, Alizadeh AM, Esmati E (2017) An agent-based model of avascular tumor growth: immune response tendency to prevent cancer development. SIMULATION 93:641–657. https://doi.org/10.1177/0037549717699072

Powathil GG, Gordon KE, Hill LA, Chaplain MA (2012) Modelling the effects of cell-cycle heterogeneity on the response of a solid tumour to chemotherapy: biological insights from a hybrid multiscale cellular automaton model. J Theor Biol 308:1–19. https://doi.org/10.1016/j.jtbi.2012.05.015

Prats C, Vilaplana C, Valls J, Marzo E, Cardona PJ, Lopez D (2016) Local inflammation, dissemination and coalescence of lesions are key for the progression toward active tuberculosis: the bubble model. Front Microbiol 7:33. https://doi.org/10.3389/fmicb.2016.00033

Qi C, Liu C, Gong J, Liu D, Wang X, Zhang P, Qin Y, Ge S, Zhang M, Peng Z, Zhou J, Lu Z, Lu M, Cao Y, Yuan J, Wang Y, Wang Z, Xue R, Peng X, Wang Y, Yuan D, Li J, Zhang X, Shen L (2024) Claudin18.2-specific CAR T cells in gastrointestinal cancers: phase 1 trial final results. Nat Med 30:2224–2234. https://doi.org/10.1038/s41591-024-03037-z

Ramakrishnan L (2012) Revisiting the role of the granuloma in tuberculosis. Nat Rev Immunol 12:352–366. https://doi.org/10.1038/nri3211

Ray JC, Flynn JL, Kirschner DE (2009) Synergy between individual TNF-dependent functions determines granuloma performance for controlling *Mycobacterium tuberculosis* infection. J Immunol 182:3706–3717. https://doi.org/10.4049/jimmunol.0802297

Renardy M, Wessler T, Blemker S, Linderman J, Peirce S, Kirschner D (2019) Data-driven model validation across dimensions. Bull Math Biol 81:1853–1866. https://doi.org/10.1007/s11538-019-00590-4

Renardy M, Joslyn LR, Millar JA, Kirschner DE (2021) To Sobol or not to Sobol? The effects of sampling schemes in systems biology applications. Math Biosci 337:108593. https://doi.org/10.1016/j.mbs.2021.108593

Ruiz-Martinez A, Gong C, Wang H, Sove RJ, Mi H, Kimko H, Popel AS (2022) Simulations of tumor growth and response to immunotherapy by coupling a spatial agent-based model with a whole-patient

quantitative systems pharmacology model. PLoS Comput Biol 18:e1010254. https://doi.org/10.1371/journal.pcbi.1010254

Sarathy JP, Zuccotto F, Hsinpin H, Sandberg L, Via LE, Marriner GA, Masquelin T, Wyatt P, Ray P, Dartois V (2016) Prediction of drug penetration in tuberculosis lesions. ACS Infect Dis 2:552–563. https://doi.org/10.1021/acsinfecdis.6b00051

Saukkonen JJ, Duarte R, Munsiff SS, Winston CA, Mammen MJ, Abubakar I, Acuna-Villaorduna C, Barry PM, Bastos ML, Carr W, Chami H, Chen LL, Chorba T, Daley CL, Garcia-Prats AJ, Holland K, Konstantinidis I, Lipman M, Battista Migliori G, Parvez FM, Shapiro AE, Sotgiu G, Starke JR, Starks AM, Thakore S, Wang SH, Wortham JM, Nahid P (2025) Updates on the treatment of drug-susceptible and drug-resistant tuberculosis: an official ATS/CDC/ERS/IDSA clinical practice guideline. Am J Respir Crit Care Med 211:15–33. https://doi.org/10.1164/rccm.202410-2096ST

Schreiber RD, Old LJ, Smyth MJ (2011) Cancer immunoediting: integrating immunity's roles in cancer suppression and promotion. Science 331:1565–1570. https://doi.org/10.1126/science.1203486

Segovia-Juarez JL, Ganguli S, Kirschner D (2004) Identifying control mechanisms of granuloma formation during *M. tuberculosis* infection using an agent-based model. J Theor Biol 231:357–376. https://doi.org/10.1016/j.jtbi.2004.06.031

Sen T, Dotsu Y, Corbett V, Puri S, Sen U, Boyle TA, Mack P, Hirsch F, Aljumaily R, Naqash AR, Sukrithan V, Karim NA (2025) Pulmonary neuroendocrine neoplasms: the molecular landscape, therapeutic challenges, and diagnosis and management strategies. Lancet Oncol 26:e13–e33. https://doi.org/10.1016/S1470-2045(24)00374-7

Silva AS, Gatenby RA (2010) A theoretical quantitative model for evolution of cancer chemotherapy resistance. Biol Direct 5:25. https://doi.org/10.1186/1745-6150-5-25

Starruss J, De Back W, Brusch L, Deutsch A (2014) Morpheus: a user-friendly modeling environment for multiscale and multicellular systems biology. Bioinformatics 30:1331–1332. https://doi.org/10.1093/bioinformatics/btt772

Swat MH, Thomas GL, Belmonte JM, Shirinifard A, Hmeljak D, Glazier JA (2012) Multi-scale modeling of tissues using CompuCell 3D. Methods Cell Biol 110:325–366. https://doi.org/10.1016/B978-0-12-388403-9.00013-8

Travis WD (2012) Update on small cell carcinoma and its differentiation from squamous cell carcinoma and other non-small cell carcinomas. Mod Pathol 25(Suppl 1):S18-30. https://doi.org/10.1038/modpathol.2011.150

Vesely MD, Kershaw MH, Schreiber RD, Smyth MJ (2011) Natural innate and adaptive immunity to cancer. Annu Rev Immunol 29:235–271. https://doi.org/10.1146/annurev-immunol-031210-101324

Von Eichborn J, Woelke AL, Castiglione F, Preissner R (2013) VaccImm: simulating peptide vaccination in cancer therapy. BMC Bioinformatics 14:127. https://doi.org/10.1186/1471-2105-14-127

Wang Z, Butner JD, Kerketta R, Cristini V, Deisboeck TS (2015) Simulating cancer growth with multiscale agent-based modeling. Semin Cancer Biol 30:70–78. https://doi.org/10.1016/j.semcancer.2014.04.001

Wang S, Liu R, Yu Q, Dong L, Bi Y, Liu G (2019) Metabolic reprogramming of macrophages during infections and cancer. Cancer Lett 452:14–22. https://doi.org/10.1016/j.canlet.2019.03.015

Wang J, Hu L, Yang X, Ye X, Ni Y, Meng M, Huang G, Zhang T, Li W, Han X, Wei Z, Dai J, Zou Z (2022) A study of microwave ablation for small cell lung cancer. J Cancer Res Ther 18:399–404. https://doi.org/10.4103/jcrt.jcrt_1965_21

Warrender C, Forrest S, Koster F (2006) Modeling intercellular interactions in early *Mycobacterium* infection. Bull Math Biol 68:2233–2261. https://doi.org/10.1007/s11538-006-9103-y

Werutsky G, Hochhegger B, Lopes De Figueiredo Pinto JA, Martinez-Mesa J, Zanini ML, Berdichevski EH, Vilas E, Da Silva VD, Tsukazan MTR, Vieira A, Fritscher LG, Hartmann L, Alba M, Sartori G, Matushita C, Bortolotto V, Do Amaral RR, Junior LCA, Zaffaroni F, Barrios CH, Debiasi M, Frietscher CC (2019) PET-CT has low specificity for mediastinal staging of non-small-cell lung cancer in an endemic area for tuberculosis: a diagnostic test study (LACOG 0114). BMC Cancer 19:5. https://doi.org/10.1186/s12885-018-5233-5

Whiteside TL (2008) The tumor microenvironment and its role in promoting tumor growth. Oncogene 27:5904–5912. https://doi.org/10.1038/onc.2008.271

Winchell CG, Nyquist SK, Chao MC, Maiello P, Myers AJ, Hopkins F, Chase M, Gideon HP, Patel KV, Bromley JD, Simonson AW, Floyd-O'sullivan R, Wadsworth M, Rosenberg JM, Uddin R, Hughes T, Kelly RJ, Griffo J, Tomko J, Klein E, Berger B, Scanga CA, Mattila J, Fortune SM, Shalek AK, Lin PL, Flynn JL (2023) CD8+ lymphocytes are critical for early control of tuberculosis in macaques. J Exp Med. https://doi.org/10.1084/jem.20230707

Woelke AL, Von Eichborn J, Murgueitio MS, Worth CL, Castiglione F, Preissner R (2011) Development of immune-specific interaction potentials and their application in the multi-agent-system VaccImm. PLoS ONE 6:e23257. https://doi.org/10.1371/journal.pone.0023257

Wong EA, Evans S, Kraus CR, Engelman KD, Maiello P, Flores WJ, Cadena AM, Klein E, Thomas K, White AG, Causgrove C, Stein B, Tomko J, Mattila JT, Gideon H, Lin PL, Reimann KA, Kirschner DE, Flynn JL (2020) IL-10 impairs local immune response in lung granulomas and lymph nodes during early *Mycobacterium tuberculosis* infection. J Immunol 204:644–659. https://doi.org/10.4049/jimmunol.1901211

Wu CY, Hu HY, Pu CY, Huang N, Shen HC, Li CP, Chou YJ (2011) Pulmonary tuberculosis increases the risk of lung cancer: a population-based cohort study. Cancer 117:618–624. https://doi.org/10.1002/cncr.25616

Wu Q, Yang Z, Nie Y, Shi Y, Fan D (2014) Multi-drug resistance in cancer chemotherapeutics: mechanisms and lab approaches. Cancer Lett 347:159–166. https://doi.org/10.1016/j.canlet.2014.03.013

Wu X, Gu Z, Chen Y, Chen B, Chen W, Weng L, Liu X (2019) Application of PD-1 blockade in cancer immunotherapy. Comput Struct Biotechnol J 17:661–674. https://doi.org/10.1016/j.csbj.2019.03.006

Wynn ML, Kulesa PM, Schnell S (2012) Computational modelling of cell chain migration reveals mechanisms that sustain follow-the-leader behaviour. J R Soc Interface 9:1576–1588. https://doi.org/10.1098/rsif.2011.0726

Yang Y, Ochando JC, Bromberg JS, Ding Y (2007) Identification of a distant T-bet enhancer responsive to IL-12/Stat4 and IFNgamma/Stat1 signals. Blood 110:2494–2500. https://doi.org/10.1182/blood-2006-11-058271

Yang Y, Liu N, Wu J, Wu Q, Zhao J, Shi Y, Shen M, Xu Z, Shi Y, Yu J, Yi P, Cheng J, Sun J, Xu Y, Wang K (2025) Intratumoral heterogeneity and potential treatment strategies in small cell lung cancer. Front Oncol 15:1657441. https://doi.org/10.3389/fonc.2025.1657441

Yoon H, Kim TS, Braciale TJ (2010) The cell cycle time of CD8+ T cells responding in vivo is controlled by the type of antigenic stimulus. PLoS ONE 5:e15423. https://doi.org/10.1371/journal.pone.0015423

Yu YH, Liao CC, Hsu WH, Chen HJ, Liao WC, Muo CH, Sung FC, Chen CY (2011) Increased lung cancer risk among patients with pulmonary tuberculosis: a population cohort study. J Thorac Oncol 6:32–37. https://doi.org/10.1097/JTO.0b013e3181fb4fcc

Zhan P, Wang J, Lv XJ, Wang Q, Qiu LX, Lin XQ, Yu LK, Song Y (2009) Prognostic value of vascular endothelial growth factor expression in patients with lung cancer: a systematic review with meta-analysis. J Thorac Oncol 4:1094–1103. https://doi.org/10.1097/JTO.0b013e3181a97e31

Zheng Y, Wang Z, Wei S, Liu Z, Chen G (2021) Epigenetic silencing of chemokine CCL2 represses macrophage infiltration to potentiate tumor development in small cell lung cancer. Cancer Lett 499:148–163. https://doi.org/10.1016/j.canlet.2020.11.034

Zhong X, Ji P & Yang L (2026) Small cell lung cancer: from immunobiological mechanisms to clinical advances. Front Immunol 17:1765497. https://doi.org/10.3389/fimmu.2026.1765497

Publisher's Note Springer Nature remains neutral with regard to jurisdictional claims in published maps and institutional affiliations.